Glucocorticoid chrono-pharmacology unveils novel targets for the cardiomyocyte-specific GR-KLF15 axis in cardiac glucose metabolism

Authors: Hima Bindu Durumutla[1#], Ashok Daniel Prabakaran[1#], Fadoua El Abdellaoui Soussi[1#], Olukunle Akinborewa[1,2], Hannah Latimer[1], Kevin McFarland[1], Kevin Piczer[1], Cole Werbrich[1], Mukesh K Jain[3], Saptarsi M Haldar[4], Mattia Quattrocelli[1,*]

[#] These Authors contributed equally

Affiliations:

[1] Molecular Cardiovascular Biology, Heart Institute, Cincinnati Children's Hospital Medical Center and Dept. Pediatrics, University of Cincinnati College of Medicine, Cincinnati, OH, USA;

[2] Department of Pharmacology, Physiology and Neurobiology, University of Cincinnati College of Medicine, Cincinnati, OH, USA;

[3] Dept Cell Biology and Biochemistry, Brown University, Providence, RI, USA;

[4] Amgen Research, South San Francisco, CA, USA; Gladstone Institutes, San Francisco, CA, USA and Dept Medicine, Cardiology Division, UCSF, San Francisco, CA, USA

*** Corresponding Author:** Mattia Quattrocelli, PhD, Molecular Cardiovascular Biology, Heart Institute, Cincinnati Children's Hospital Medical Center, 240 Albert Sabin Way T4.676, Cincinnati, OH 45229. Email: mattia.quattrocelli@cchmc.org, tel: +1-513-517-1221.

Keywords – Glucocorticoids, prednisone, chrono-pharmacology, glucose uptake, pyruvate oxidation, Adipor1, mitochondrial pyruvate carrier, glucocorticoid receptor, KLF15.

Word count (including title page, full text, references, figure legends) – 11110 words.

Author contributions – HBD, ADP, FEAS, HBD, HL, KMF, KM, KP, CW: Data curation, Formal analysis, Investigation; MKJ, SMH: Resources; MQ: Conceptualization, Formal analysis, Funding acquisition, Supervision. Order of co-first Authors was assigned based on overall weight of contribution considering initial and revised submissions.

Conflicts of interest – MQ is listed as co-inventor on a patent application related to intermittent glucocorticoid use filed by Northwestern University (PCT/US2019/068,618). All other authors declare they have no competing interests.

Brief summary – Depending on when it is taken during the day, the drug prednisone activates the heart to consume glucose to produce energy.

38 **GRAPHICAL ABSTRACT**

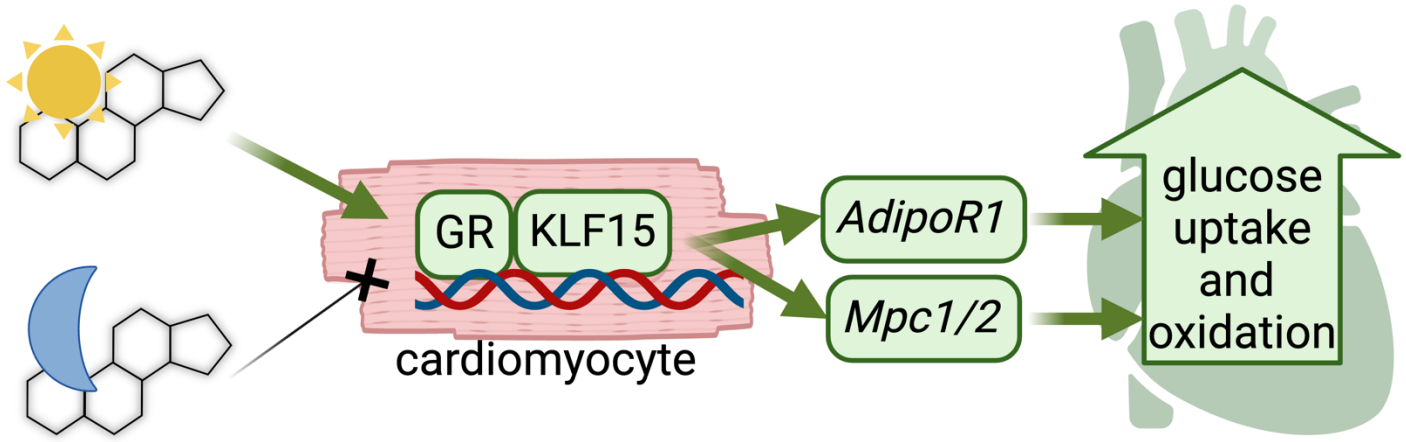

39
40
41

42 **ABSTRACT**

43 Circadian time-of-intake gates the cardioprotective effects of glucocorticoid administration in both healthy and
44 infarcted hearts. The cardiomyocyte-specific glucocorticoid receptor (GR) and its co-factor, Krüppel-like factor
45 (Klf15), play critical roles in maintaining normal heart function in the long-term and serve as pleiotropic regulators
46 of cardiac metabolism. Despite this understanding, the cardiomyocyte-autonomous metabolic targets influenced
47 by the concerted epigenetic action of GR-Klf15 axis remain undefined. Here, we demonstrate the critical roles of
48 the cardiomyocyte-specific GR and Klf15 in orchestrating a circadian-dependent glucose oxidation program
49 within the heart. Combining integrated transcriptomics and epigenomics with cardiomyocyte-specific inducible
50 ablation of GR or Klf15, we identified their synergistic role in the activation of adiponectin receptor expression
51 (*Adipor1*) and the mitochondrial pyruvate complex (*Mpc1/2*), thereby enhancing insulin-stimulated glucose
52 uptake and pyruvate oxidation. Furthermore, in obese diabetic (*db/db*) mice exhibiting insulin resistance and
53 impaired glucose oxidation, light-phase prednisone administration, as opposed to dark-phase prednisone
54 dosing, effectively restored cardiomyocyte glucose oxidation and improved diastolic function towards control-like
55 levels in a sex-independent manner. Collectively, our findings uncover novel cardiomyocyte-autonomous
56 metabolic targets of the GR-Klf15 axis. This study highlights the circadian-dependent cardioprotective effects of
57 glucocorticoids on cardiomyocyte glucose metabolism, providing critical insights into chrono-pharmacological
58 strategies for glucocorticoid therapy in cardiovascular disease.

59

INTRODUCTION

Chronic elevation of glucose levels in diabetes leads to pathological changes in mammalian cells, culminating in cellular and tissue damage, particularly affecting the cardiovascular system. Cardiovascular complications stand as the primary cause of morbidity and mortality among patients with diabetes mellitus (1). Moreover, individuals with metabolic disorders such as obesity and type-2 diabetes (T2D) are predisposed to diabetic cardiomyopathy, a condition of metabolic heart failure (2). T2D imposes metabolic stress on the heart, manifesting in – among others - two major defects: insulin resistance and impaired glucose oxidation. Insulin resistance in glucose uptake constitutes a critical metabolic insult in diabetic hearts and promotes a substrate imbalance that exacerbates diastolic dysfunction, i.e. loss of glucose oxidation with dominating lipid oxidation (3, 4). Moreover, the accumulation of ceramides in the diabetic myocardium further promotes a lipotoxic effect, compromising insulin sensitivity and glucose uptake (5). While previous studies have addressed the deficits in glucose oxidation and insulin sensitivity as single lines of action, comprehensive strategies to manage the metabolic abnormalities in diabetic cardiomyopathy remain elusive. Despite advancements in therapeutics approaches, including SGLT2 inhibitors and GLP1 agonists and/or lifestyle interventions, cardiovascular disease remains a leading cause of morbidity and mortality, accounting for ~40% of deaths in diabetic patients (6) – a statistic that continues to rise every year. Here we report a completely unanticipated role for the glucocorticoid receptor (GR) and its co-factor Krüppel-like factor 15 (Klf15) in regulating insulin-sensitive glucose uptake and oxidation in heart, addressing a critical clinical need to mitigate cardiovascular morbidity in these patients.

The glucocorticoid receptor (GR) is a potent metabolic regulator that acts as transcription factor when activated by glucocorticoids. The cardiomyocyte-specific GR is important for heart function (7), but the cardiomyocyte-autonomous role of GR in heart metabolism remains unknown. Notably, the glucocorticoid-GR axis is tightly linked to the circadian rhythm (8) and we previously reported that circadian time-of-intake gates the cardioprotective program enabled by the glucocorticoid in heart in a cardiomyocyte-autonomous, clock-dependent way (9). Among its targets, the GR activates its co-factor KLF15 (10), which regulates cardiac metabolism (11) and promotes circadian transcriptional programs in heart (12). However, direct metabolic targets of the GR-KLF15 axis in cardiomyocytes are still remarkably unknown. Here we combine chrono-pharmacology with cardiomyocyte-specific inducible ablation and RNA-seq/ChIP-seq datasets to identify *Adipor1* and *Mpc1/2*

87 as novel critical targets of GR and KLF15 in cardiac glucose utilization. Furthermore, we tested the relevance of
88 these chrono-pharmacology targets for cardiac glucose oxidation and diastolic dysfunction improvements in
89 obese diabetic mice. Our findings challenge the current paradigms in glucocorticoid biology and identify novel
90 druggable mechanisms underlying the interplay between GR and KLF15. These insights may offer potential
91 therapeutic strategies to combat metabolic inflexibility in heart failure.

92

93

RESULTS

Light-phase dosing gates the glucocorticoid effects on cardiomyocyte glucose metabolism.

In our previous study, we reported that the cardioprotective circadian effects of the glucocorticoid prednisone in infarcted murine hearts are gated by the circadian time-of-intake (9). To elucidate the underlying molecular mechanisms, we analyzed RNA-seq datasets from uninjured (sham-operated) and myocardial tissues (GSE186875). Our analysis revealed that intermittent prednisone administration (once-weekly i.p. 1mg/kg for 12 weeks) at Zeitgeber time 0 (ZT0, lights-on) significantly upregulated genes associated with increased glucose import and pyruvate transport pathways compared to vehicle controls. Amongst the genes involved in these pathways, we observed a remarkable upregulation of *Klf15*, *Adipor1* and *Mpc1/2* following ZT0 prednisone stimulation **(Figure 1A)**. Klf15 is a known circadian metabolic regulator of nutrient flux in the heart (12-15), yet its specific targets in conjunction with its co-factor GR (16) remain unknown. *Adipor1* encodes the adiponectin-activated ceramidase that is sufficient to promote insulin-sensitive glucose uptake (17, 18); *Mpc1/2* encode the two subunits of the mitochondrial pyruvate carrier, essential for cardioprotective pyruvate oxidation (19-21). To test whether the steroid-driven transactivation of these genes was dependent on time-of-day, we treated *wild-type* C57BL/6J males with 12-week-long intermittent prednisone treatments at ZT0 versus ZT12, i.e. at start of light-phase vs start of dark-phase **(Supplemental Figure 1A).** Consistent with our RNAseq data, qPCR analysis showed that ZT0 prednisone significantly increased *Klf15, Adipor1, Mpc1 and Mcp2* compared to vehicle and, notably, the drug effect was significantly lower or blunted with ZT12 injections **(Figure 1B)**. While we reported that circadian time of prednisone dosing did not change overall protein levels or nuclear translocation capacity of the GR in heart (9), we were intrigued by the time-of-dosing effects on *Klf15* expression. As KLF15 physically binds the GR as co-activator (16), we tested the extent to which the time-specific gating on *Klf15* upregulation converted in a parallel chrono-pharmacological effect on GR-KLF15 protein-protein interaction. At 4hrs after last drug dose, we found that indeed KLF15 binding to GR was increased by ZT0 prednisone to a higher extent than what shown by ZT12 prednisone **(Figure 1C)**. To assess the functional implications of *Adipor1, Mpc1 and Mcp2* upregulation in cardiac metabolic remodeling, we quantitated myocardial ceramide abundance through mass-spectrophotometry; glucose uptake through 2-deoxyglucose (2DG) assay *in vivo*; glucose oxidation through glucose-fueled respirometry in isolated cardiomyocytes and pyruvate-fueled respiratory control ratio (RCR) (22)

121 in myocardial-derived isolated mitochondria, analyzing data as aggregated **(Figure 1C-F)** and disaggregated by
122 sex **(Figure S1B-E)**. In line with *Adipor1* upregulation, ZT0 but not ZT12 prednisone decreased myocardial
123 ceramides **(Figure 1C)**. With ZT0 prednisone administration, we observed a significant increase in insulin-
124 dependent 2DG uptake **(Figure 1D)**, glucose-fueled respiration, and calculated ATP production in
125 cardiomyocytes **(Figure 1E)**. Consistent with the upregulation of *Mpc1/2*, ZT0 treatment also elevated ADP-
126 stimulated respiration in mitochondria, increasing pyruvate-fueled RCR **(Figure 1F)**. Ceramide clearance and
127 the effects in cardiomyocytes and mitochondria were sex-independent **(Figure S1B-E)**. Regarding the gene
128 expression trends, we sought to gain insight in expression oscillations and time-of-intake effects in heart. We
129 performed a circadian time-course qPCR analysis in myocardial tissues after a single prednisone pulse at ZT0
130 vs ZT12, to compare circadian trends in the absence of chronic secondary effects. Expression curves revealed
131 oscillations of variable amplitude for *Klf15, Adipor1 and Mpc1/2* in the wild-type myocardium, with the most
132 pronounced circadian mRNA acrophases for *Klf15* in the light-phase and *Mpc1* during the light-dark phase
133 transition **(Figure 1G)**. The transactivation effect by a single prednisone pulse was pronounced and prolonged
134 over the circadian cycle with ZT0 injections, while ZT12 prednisone effects were either transient or non-significant
135 **(Figure 1G)**. Considering the upregulation of *Klf15* appeared central in the circadian-specific prednisone-GR
136 program, we asked whether the cardiomyocyte clock was mediating the time-specific effect. Indeed, we
137 previously showed that the cardiomyocyte-specific BMAL1 was required for the ZT0 prednisone-specific pro-
138 energetic effects in heart (9). Following the ChIP-seq indications of GR-BMAL1 interplay previously garnered in
139 muscle (23), we looked for GR elements (GRE; ACAnnnTGT) and BMAL1 E-Box sites (CACGTG) in the *Klf15*
140 proximal promoter within 300-900bp from each other and found a proximal promoter region with GRE and E-Box
141 at ~600bp from each other **(Supplemental Figure 1F)**. Through ChIP-qPCR in myocardial tissue at 4hrs after
142 last drug injection, we found that GR occupancy on the GRE was increased by treatment regardless of time-of-
143 intake, while BMAL1 occupancy on the E-Box was increased specifically by ZT0 and not ZT12 prednisone
144 **(Supplemental Figure 1F).** We leveraged the mice with inducible cardiomyocyte-specific BMAL1-KO we
145 previously reported (9) to assess the extent to which BMAL1 was required for the ZT0 prednisone effect on
146 cardiac *Klf15* transactivation. After tamoxifen and washout following prior conditions (9), BMAL1-KO vs BMAL1-
147 WT littermates were treated with 12-week-long ZT0 prednisone or vehicle treatments. In heart, cardiomyocyte
148 BMAL1 ablation blocked the ZT0 prednisone effects on GR occupancy of the Klf15 promoter GRE and on Klf15

149 mRNA upregulation. The data were further validated by parallel analyses in skeletal muscle, where BMAL1 was
150 not ablated and ZT0 prednisone effects were indeed not blocked **(Supplemental Figure 1G).** Taken together,
151 our findings indicate that circadian time-of-intake gates the prednisone effects on *Klf15, Adipor1 and Mpc1/2*
152 oscillations, as well as ceramide clearance, insulin-sensitive glucose uptake and pyruvate oxidation in the
153 uninjured heart.

154 ***Generation of ChIP-seq and RNA-seq datasets for the cardiomyocyte-autonomous GR and KLF15.***
155 Given the expected upregulation of *Klf15* and activation of GR by prednisone treatment, we tested the role of
156 the GR-Klf15 axis in mediating the upregulation of *Adipor1* and *Mpc1/*2 by light-phase glucocorticoids specifically
157 in cardiomyocytes. For this we sought to garner unbiased evidence of GR and KLF15 epigenomic occupancy
158 and transcriptional effects in heart. To profile epigenomic occupancy of GR and Klf15 in myocardial tissue, we
159 conducted parallel chromatin immunoprecipitation sequencing (ChIP-seq) experiments at 4 hours after a single
160 pulse of ZT0 prednisone administration, adapting the method reported for muscle in our previous study (24). We
161 focused on epigenomic shifts after single drug pulse to avoid secondary effects of chronic drug administration.
162 Notably, due to the lack of ChIP-seq-grade commercial antibodies for Klf15, we performed the
163 immunoprecipitations in myocardial tissue of Klf15-3xFLAG$^{+/-}$ knock-in mice, which were previously reported
164 (25). Our unbiased motif analysis validated the specificity of GR and Klf15 immunoprecipitations, revealing high
165 enrichment for each factor's canonical binding motifs **(**glucocorticoid response elements, GREs; KLF response
166 elements, KREs; **Figure 2A)**. The epigenomic activity of both GR and Klf15 was activated by ZT0 prednisone in
167 myocardium, as indicated by increased peak number and signal intensity over canonical sites genome-wide
168 **(Figure 2B)**. However, there were no discernible drug-induced changes in peak localization, which remained
169 highly enriched in promoter-transcriptional start sites (TSS) **(Figure 2B)**.
170 Next, to gain proof of requirement for target gene expression trends, we collected RNA-seq datasets from hearts
171 of cardiomyocyte-specific inducible knockout (*KO*) versus wild-type (*WT*) mice for each factor, using the same
172 tamoxifen and washout protocol **(Figure S2A)**. For GR-KO we used the mice we previously reported (9),
173 comparing hearts from *Myh6-MerCreMer*$^{+/-}$*;Nr3c1*$^{fl/fl}$ (*GR-KO*) versus *Myh6-MerCreMer*$^{+/-}$*;Nr3c1*$^{wt/wt}$ (*GR-WT*)
174 mice. Similarly, for *Klf15-KO* mice we compared *Myh6-MerCreMer*$^{+/-}$*;Klf15*$^{fl/fl}$ (*KLF15-KO*) versus *Myh6-*
175 *MerCreMer*$^{+/-}$*;Klf15*$^{wt/wt}$ (*KLF15-WT*) **(Supplemental Figure 2B**), using the previously reported *Klf15-floxed* allele

176 (12). As for the ChIP-seq datasets, the RNA-seq datasets were garnered from hearts collected at 4 hours after
177 a single ZT0 prednisone pulse. Principal component analysis (PCA) of the RNA-seq datasets clustered samples
178 based on drug treatment and cardiomyocyte genotype for either *GR* or *Klf15* **(Fig 2C)**, suggesting a non-
179 redundant requirement for both factors in the transcriptional program enabled by ZT0 prednisone in heart. We
180 therefore generated datasets to unbiasedly probe the extent to which the cardiomyocyte-specific GR-KLF15 axis
181 regulates *Adipor1 and Mpc1/2* expression in heart.
182
183 ***Cardiomyocyte GR and Klf15 are independently required for the ZT0 prednisone effect on Adipor1 and***
184 ***Mpc1/2 transactivation, insulin-driven glucose uptake and pyruvate oxidation.***
185 We first tested the extent to which *Adipor1* was a direct transactivation target of GR and Klf15 in heart
186 downstream of ZT0 prednisone. ChIP-seq peak tracks revealed steroid-sensitive peaks on the *Adipor1* proximal
187 promoter for both GR and Klf15. RNA-seq data showed that the inducible cardiomyocyte-specific ablation of
188 either GR or Klf15 blocked the drug-induced upregulation of *Adipor1*, indicating a non-redundant requirement for
189 both factors in a cardiomyocyte-autonomous fashion **(Figure 3A)**. Based on the motifs unveiled by the unbiased
190 motif analysis of ChIP-seq datasets (ACAnnnTGT for GRE; GGGCGGGG for KRE), we found GRE and KRE
191 motifs in the proximal promoter of *Adipor1* and validated the ChIP-seq and RNA-seq indications through ChIP-
192 qPCRs and qPCRs **(Supplemental Figure 2C)**. In accordance with the trends in *Adipor1* transactivation,
193 cardiomyocyte-specific inducible ablation of either GR or Klf15 blocked the chronic ZT0 prednisone effects on
194 ceramide reduction and 2DG uptake in heart. The transcriptional and metabolic effects of treatment appeared
195 durable and extended to not only the light-phase, but also the active phase of treated mice **(Figure 3B;**
196 **Supplemental Figure 2C)**. Similarly, we found steroid-sensitive peaks on the proximal promoters of *Mpc1* and
197 *Mpc2*, with ZT0 prednisone transactivation of both genes blocked by cardiomyocyte-specific ablation of either
198 GR or Klf15 **(Figure 3C)**. We found GRE and KRE motifs in the 5' UTRs of both *Mpc1* and *Mpc2* and validated
199 GR-KLF15 occupancy and gene upregulation through ChIP-qPCRs and qPCRs **(Supplemental Figure 2C)**. In
200 accordance with the trends in *Mpc1/2* transactivation, the chronic treatment-driven gain in pyruvate oxidation
201 was also blocked by the inducible gene and the KLF15-dependent chronic treatment effects were applicable to
202 both active and rest phase of mice (**Figure 3D; Supplemental Figure 2D**). Taken together, these findings

203 demonstrate that the ZT0-specific prednisone stimulation of glucose uptake and oxidation in heart is mediated
204 by the cardiomyocyte-autonomous epigenetic activity of both GR and Klf15.
205 We then assessed heart function through echocardiography in our cohorts at start and end of 12-week-long ZT0
206 prednisone treatments. We primarily focused on fractional shortening, stroke volume and heart weight/tibia
207 length, as those parameters were previously shown to be impacted by both GR and KLF15 constitutive (post-
208 natal, not inducible) ablations in heart (26, 27). In our own mice after inducible ablation and in the absence of
209 prednisone, KO for either factor significantly depressed fractional shortening and stroke volume, while increasing
210 heart mass, when compared to WT controls. In WT uninjured hearts, ZT0 prednisone treatment increased stroke
211 volume and fractional shortening, with no significant trends in normalized heart weight. As expected, treatment
212 had no sizable effects in KO hearts **(Figure 4)**. In line with the trends in fractional shortening and stroke volume,
213 KO for either factor enlarged the systolic left ventricle diameter (LVIDs) and induced non-significant declines in
214 ejection fraction and gains in diastolic left ventricle diameter (LVIDd). In WT hearts, treatment induced a small
215 significant reduction of LVIDs, a non-significant trend in increased ejection fraction and no appreciable changes
216 in LVIDd. In KO hearts, treatment had no sizable effects. Heart rate during the echocardiographic measurements,
217 i.e. under anesthesia, was not changed by either KO or treatment **(Supplemental Figure 3)**. Therefore, inducible
218 ablation of either GR or KLF15 after normal growth recapitulated the constitutive post-natal ablation effects on
219 uninjured heart, blocking the treatment-driven gains in stroke volume.
220

221 ***Light-phase glucocorticoid intermittence rescues glucose oxidation and diastolic dysfunction in***
222 ***diabetic hearts.***
223 We hypothesized that combining the ZT0 prednisone effects on insulin sensitization and pyruvate oxidation could
224 serve as a "two-hit" approach to enhance a functional glucose oxidation program in the diabetic heart. Given that
225 insulin resistance and impaired glucose oxidation are key metabolic dysfunctions in T2D diabetic cardiomyopathy
226 (3, 4), we aimed to evaluate the relevance of this ZT0 prednisone program in a diabetic cardiomyopathy model.
227 To address this, we employed 6-month-old *db/db* obese diabetic mice (**Figure 5A**) (28, 29) and their *db/+*
228 littermates as non-obese, non-diabetic parallel control cohort. At baseline, we reconfirmed previously reported
229 defects in diastolic function (mitral valve flow impairment and increased E/e' (29)), systolic function (decreased

230 stroke volume (30, 31)) and cardiac hypertrophy (increased heart mass to tibia length (32)) in *db/db* mice vs *db/+*
231 controls **(Figure 5B)**. Importantly, these parameters were rescuable in *db/db* mice through experimental
232 interventions re-activating glucose uptake and oxidation (30-33). After treatment with intermittent prednisone at
233 ZT0 versus ZT12 for 12 weeks, ZT0 prednisone alleviated diastolic dysfunction, stroke volume impairment and
234 cardiac hypertrophy in *db/db* mice towards control *db/+* levels, while the treatment effects were blocked by ZT12
235 injections **(Figure 5C-E)**. Only with ZT0 dosing did treatment increase glucose uptake in myocardial tissue,
236 measured as 2DG uptake, in both *db/+* and *db/db* hearts **(Figure 5F)**. Also, compared to isochronic vehicle, ZT0
237 but not ZT12 prednisone treatment increased glucose-fueled basal respiration and ATP production in *db/db*
238 cardiomyocytes towards control-like control *db/+* levels (**Figure 5F**). Notably, none of these parameters showed
239 significant sexual dimorphism in their effects (**Supplemental Fig 4A**). Treatments had no sizable effects on body
240 weight beyond the expected genotype-dependent increase **(Supplemental Figure 4B)**. Furthermore, we
241 checked blood pressure through tail cuff measurements on the day after the last injection, considering the
242 hypertensive phenotype of db/db mice (34) and the hypertensive potential of chronic glucocorticoid treatments
243 (35). We conducted the tail cuff measurements in the active phase (ZT16) to avoid potential confounding dips
244 induced by sleep or rest. None of the treatments had sizable effects on blood pressure or heart rate during blood
245 pressure measurements beyond the expected db/db-related mild hypertension in both systole and diastole
246 (**Supplemental Fig 4C**). In light of the ZT0-specific effects of prednisone on KLF15-GR interaction in WT non-
247 diabetic hearts, we tested the extent to which the chronic ZT0 vs ZT12 regimens changed GR or KLF15 nuclear
248 translocation in db/db hearts. We performed WB for GR and KLF15 in db/db myocardial lysate fractions at 30min
249 after the last injection of ZT0 vs ZT12 prednisone at the end of the 12-week-long treatment. We found that time-
250 of-intake did not sizably change the rate of GR nuclear translocation, while it did impact KLF15 translocation,
251 which was specifically increased by ZT0 prednisone **(Supplemental Figure 5A)**. Indeed, in line with the model
252 of GR-KLF15 transactivation of AdipoR1 and MPC1/2, we found that at 24hrs after last drug injection those
253 proteins were increased by ZT0 prednisone – but not ZT12 prednisone – compared to vehicle in db/db hearts
254 **(Supplemental Fig 5B)**. We also found analogous trends in the glucose transporters GLUT1 and GLUT4
255 **(Supplemental Fig 5B)**, which were convergent with the glucose uptake reactivation in those hearts and
256 consistent with prior seminal findings with KLF15 overexpression (36). Finally, we sought to validate that the ZT0
257 prednisone effects in db/db hearts were dependent on GR and KLF15. To that goal, we used MyoAAV-serotyped

258 vectors containing either a scramble or anti-*Nr3c1* (MyoAAV-antiGR) or anti-*Klf15* (MyoAAV-antiKLF15) shRNA
259 under the U6 promoter. The MyoAAV serotype maximizes tropism of transduction for AAV vectors in vivo to
260 striated muscles (37). To maximize knockdown, three different vectors each with a different shRNA were
261 combined per gene knockdown. At 6 months of age, male db/db mice were injected r.o. with $6x10^{12}$ vg/mouse
262 MyoAAV-scramble or 10^{12} vg/mouse/vector MyoAAV-antiGR (3 vectors) + MyoAAV-antiKLF15 (3 vectors)
263 immediately before starting the 12-week-long ZT0 prednisone vs vehicle intermittent regimens. At endpoint, WB
264 in myocardial tissue confirmed GR and KLF15 knockdown (approximately ~80% protein reduction) and showed
265 that the knockdown vectors blocked or blunted the ZT0 prednisone effects on upregulation of Adipor1, Mpc1/2
266 protein levels in db/db hearts **(Figure 6A)**. Accordingly, the combinatorial GR+KLF15 knockdown blocked the
267 treatment effects on diastolic dysfunction (E/e'), stroke volume, cardiac hypertrophy (heart weight/tibia length)
268 and insulin-driven glucose uptake (2DG6P; **Figure 6B-C**). Moreover, treatment increased glucose-fueled
269 respiration (oxygen consumption rate, OCR) in permeabilized cardiac biopsies and pyruvate-fueled respiration
270 (respiratory control ratio, RCR) in isolated myocardial mitochondria in scramble- but not knockdown-transduced
271 hearts **(Figure 6D)**. Taken together, these data indicate the potential for prednisone chrono-pharmacology to
272 reactivate glucose oxidation and alleviate dysfunction in obese diabetic hearts by engaging the GR-KLF15
273 interplay in heart in vivo.
274
275
276

DISCUSSION

The GR plays a pivotal role in metabolic regulation, acting as a transcription factor when activated by glucocorticoids. While the importance of cardiomyocyte-specific GR in heart function is recognized (7), its autonomous role in heart metabolism remains unclear. Our previous work has elucidated two critical time dimensions influencing the outcomes of GR activation: i) circadian time-of-intake and ii) chronic frequency-of-intake. Light-phase dosing of prednisone in mice has shown benefits in heart function compared to dark-phase dosing (9). Intermittent once-weekly dosing reversed the dysmetabolic effects of chronic daily dosing and improved exercise tolerance (38). In obese diabetic mice, endogenous glucocorticoids are elevated in response to metabolic stress and yet they maintain circadian oscillations, albeit dimmed (39). This will be an important point to elucidate for the translation of our findings into pharmacological strategies for diabetic cardiomyopathy, although pilot clinical data with prednisone chrono-pharmacology in patients with muscular dystrophies showed promising improvements in lean mass and exercise tolerance (40).

Despite the known regulation of GR activity by the circadian clock (41, 42), the specific targets of glucocorticoid chrono-pharmacology for functional cardiac metabolic remodeling remain poorly elucidated. Our findings from this study discover one such mechanism: the cardiomyocyte-autonomous requirement for the GR-KLF15 axis in facilitating light-phase-specific glucocorticoid transactivation of Adipor1 and the MPC complex genes in the heart. Adipor1, an adiponectin-responsive ceramidase (43) is generally linked to pro-metabolic effects and plays a crucial role in insulin-sensitive glucose uptake by degrading ceramides (18, 44). Ceramides accumulate in heart with obesity and/or T2D, promoting cardiac insulin resistance and the related cardiac dysfunction (45). It is important to note that overt, unbalanced reactivation of glucose uptake in the insulin resistant heart causes unwanted side effects, as shown by cardiomyocyte GLUT4 overexpression in diabetic hearts (46). In that perspective, our findings with the simultaneous upregulation of both Adipor1 and the MPC complex could offer a model to reactivate both glucose uptake and downstream oxidation in a balanced fashion.

MPC expression is downregulated in failing human hearts (47) and transcriptional MPC abundance directly promotes cardioprotective oxidation of pyruvate and its precursor glucose in the myocardium (19, 20, 47). Accordingly, MPC activity is decreased in the diabetic heart too (48). It was remarkable to observe a strong

304 concerted epigenetic program by the cardiomyocyte-specific GR and Klf15 on both subunit genes for the MPC,
305 which indeed resulted in pyruvate oxidation trends in line with increased glucose oxidation.
306 The variable of circadian time of drug intake inevitably questions the time gating on not only basic mechanisms
307 but also chronic effects with respect to the circadian cycle. Here, the ZT0-prednisone-gated interaction between
308 GR and KLF15 stimulated cardiomyocyte-autonomous transcriptional/metabolic effects that extended to both
309 rest- and active-phases of mice after chronic treatment. In other words, a repetitive series of circadian-specific
310 drug stimulations supported a virtuous program that improved glucose handling in cardiomyocytes throughout
311 the circadian cycle. This is an emerging aspect in various contexts of chrono-pharmacology, including the
312 heterogenous landscape of chrono-immunology for cardiovascular health (49). Particularly in the context of
313 diabetic cardiomyopathy, these findings open the question for future studies of which chrono-regimens can be
314 complemented to concertedly leverage the endogenous rhythms of all the critical cell compartments of the heart,
315 including cardiomyocytes, fibroblasts, endothelium and immune cells.
316 **Limitations of the study –** While sufficiently powered for overall trends with chrono-treatments and gene
317 ablation, our cohort numbers were limited and likely underpowered for omics analyses and sex-specific
318 differences. The limited numbers used for RNA-seq and ChIP-seq were mitigated by dataset overlay and
319 further validation through two different cardiomyocyte-specific inducible KO models. The limited numbers of
320 mice in our sex-disaggregated analyses probably limited the detection of sexual dimorphism, which will have to
321 be addressed for the pathways in play here with appropriate cohort numbers and hormonal manipulations in
322 future studies. Despite the mechanistic evidence offered by cardiomyocyte-specific GR and KLF15 inducible
323 ablation in non-diabetic conditions and by the in vivo knockdown in db/db hearts, in this study we did not
324 directly address the requirement for the effects on insulin sensitivity and glucose oxidation per se in the
325 metabolic remodeling of the obese diabetic heart. We believe this is beyond the scope of this investigation.
326 **Conclusions and overall impact –** In summary, our study challenges the current paradigm of glucocorticoid
327 cardiotoxicity by identifying a specific mechanism that mediates the circadian-gated glucocorticoid benefit on
328 cardiomyocyte glucose oxidation, with functional implications for diabetic cardiomyopathy.
329

330

Acknowledgements - Mass-spec analyses were performed at the Cincinnati Children's Mass-Spec (Clinical and Biomedical) Facility (RRID: SCR_022638), with critical assistance by Drs. Setchell and Zhao. Next-gen sequencing was performed at the Cincinnati Children's DNA Sequencing and Genotyping Facility (RRID: SCR_022630), with critical assistance by David Fletcher, Keely Icardi, Julia Flynn, and Taliesin Lenhart.

Grant support – This work was supported by R01HL166356-01, R03DK130908-01A1, R01AG078174-01 (NIH) and RIP, GAP, CCRF Endowed Scholarship, HI Translational Funds (CCHMC) grants to MQ.

Figures

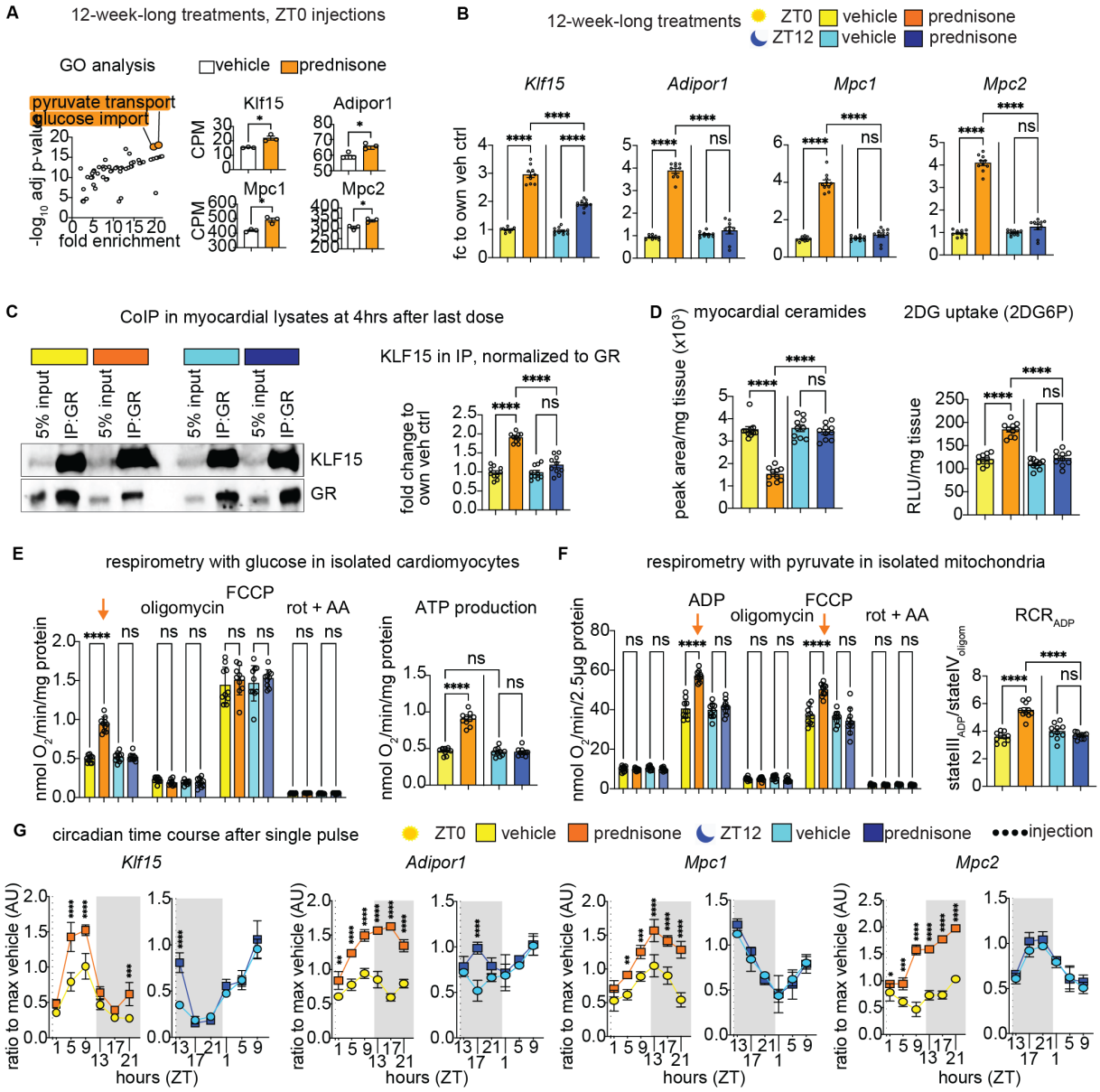

Figure 1. Light-phase glucocorticoid stimulation improves glucose uptake and oxidation in the heart. (A) Gene Ontology (GO) analysis revealed that ZT0 intermittent prednisone increased expression of *Klf15*, *Adipor1*, *Mpc1* and *Mpc2* from the enriched pathways of pyruvate transport and glucose import in the wild-type hearts. **(B)** Upregulation of Klf15 by prednisone was higher after ZT0 than ZT12 dosing, and upregulation of *Adipor1*, *Mpc1* and *Mpc2* was specific to ZT0 and blunted by ZT12 dosing. **(C)** CoIPs in heart tissue showed that KLF15 interaction with GR was higher with ZT0 than ZT12 prednisone. **(D)** Consistent with *Adipor1* upregulation, ZT0 prednisone treatment decreased myocardial ceramide levels and increased insulin-dependent 2DG uptake in heart. **(E)** After ZT0 treatment, cardiomyocytes increased basal glucose-fueled respiration ex vivo (arrow), producing more ATP than control or ZT12 treatment. **(F)** Consistent with *Mpc1/2* upregulation, ZT0 treatment increased ADP-stimulated respiration (arrow) and respiratory control ratio with pyruvate. **(G)** Circadian time-course qPCR analyses in myocardial tissues revealed oscillations of variable amplitude for *Klf15*, *Adipor1* and *Mpc1/2* expression. The transactivation effect by a single prednisone pulse was pronounced and prolonged over the circadian cycle with ZT0 injections, while ZT12 prednisone effects were either transient or non-significant. Shown are mean±S.E.M, histograms show also individual mouse values. n=3♂/group in A, n=(5♀+5♂)/group in B-G; A: Welch's t-test; B-H: 2w ANOVA + Sidak; *, P<0.05; **, P<0.01; ***, P<0.001; ****, P<0.0001.

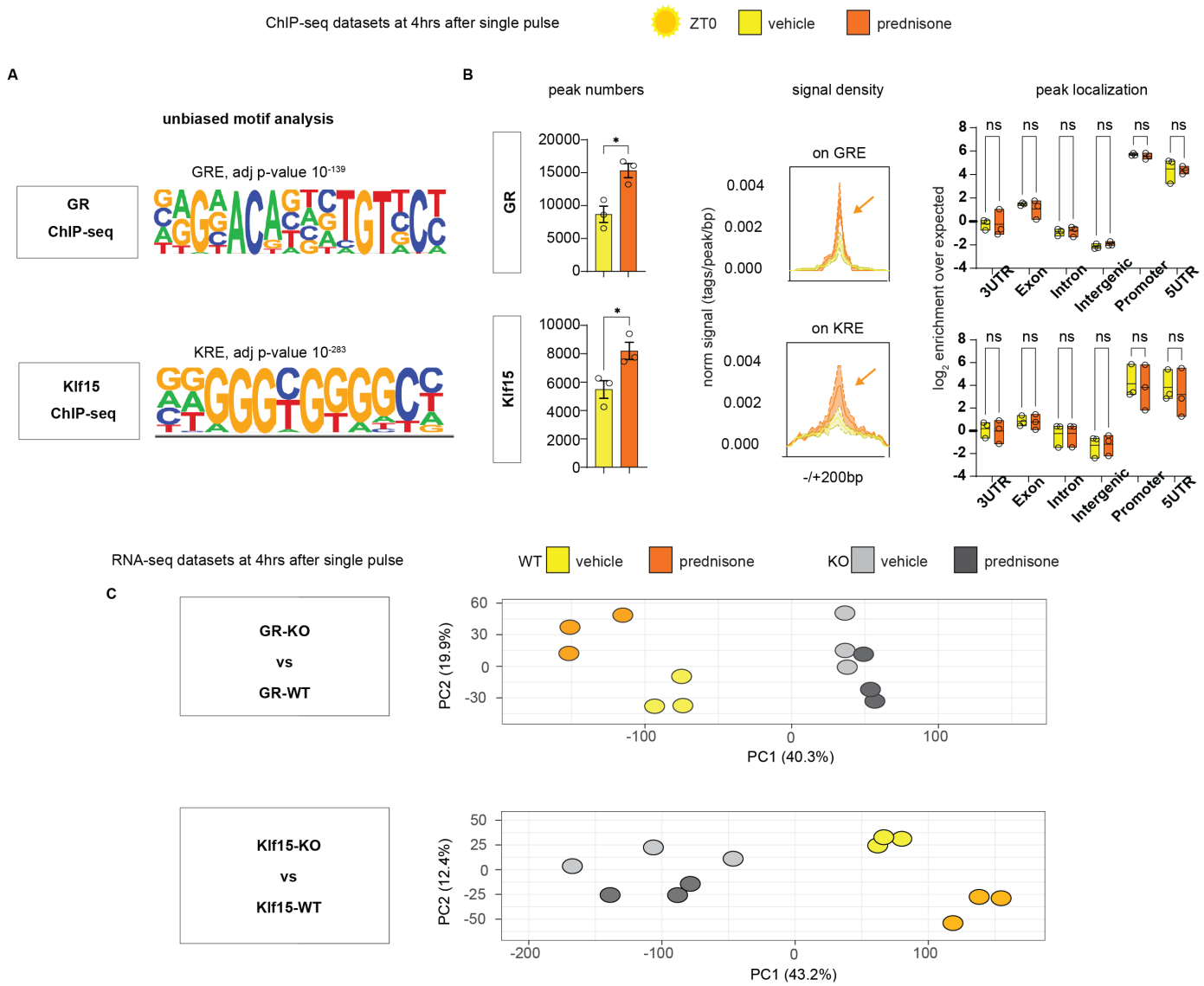

Figure 2. ChIP-seq and RNA-seq datasets reveal non-redundant mediator effect of both cardiomyocyte-specific GR and Klf15 on ZT0 glucocorticoid gene programs in heart. (A) Validation of ChIP-seq datasets through unbiased motif analysis. **(B)** Prednisone increased peak numbers and canonical epigenomic peak signal (arrows) for both GR and KLF15 without changes in relative enrichment in genomic localization, which was enriched in promoter and 5'UTRs for both factors. **(C)** PCA analyses show sample clustering according to drug and genotype variables. n=3♂/group; B-D: peak number, Welch's t-test; peak localization, 2w ANOVA + Sidak; *, P<0.05; **, P<0.01; ***, P<0.001; ****, P<0.0001.

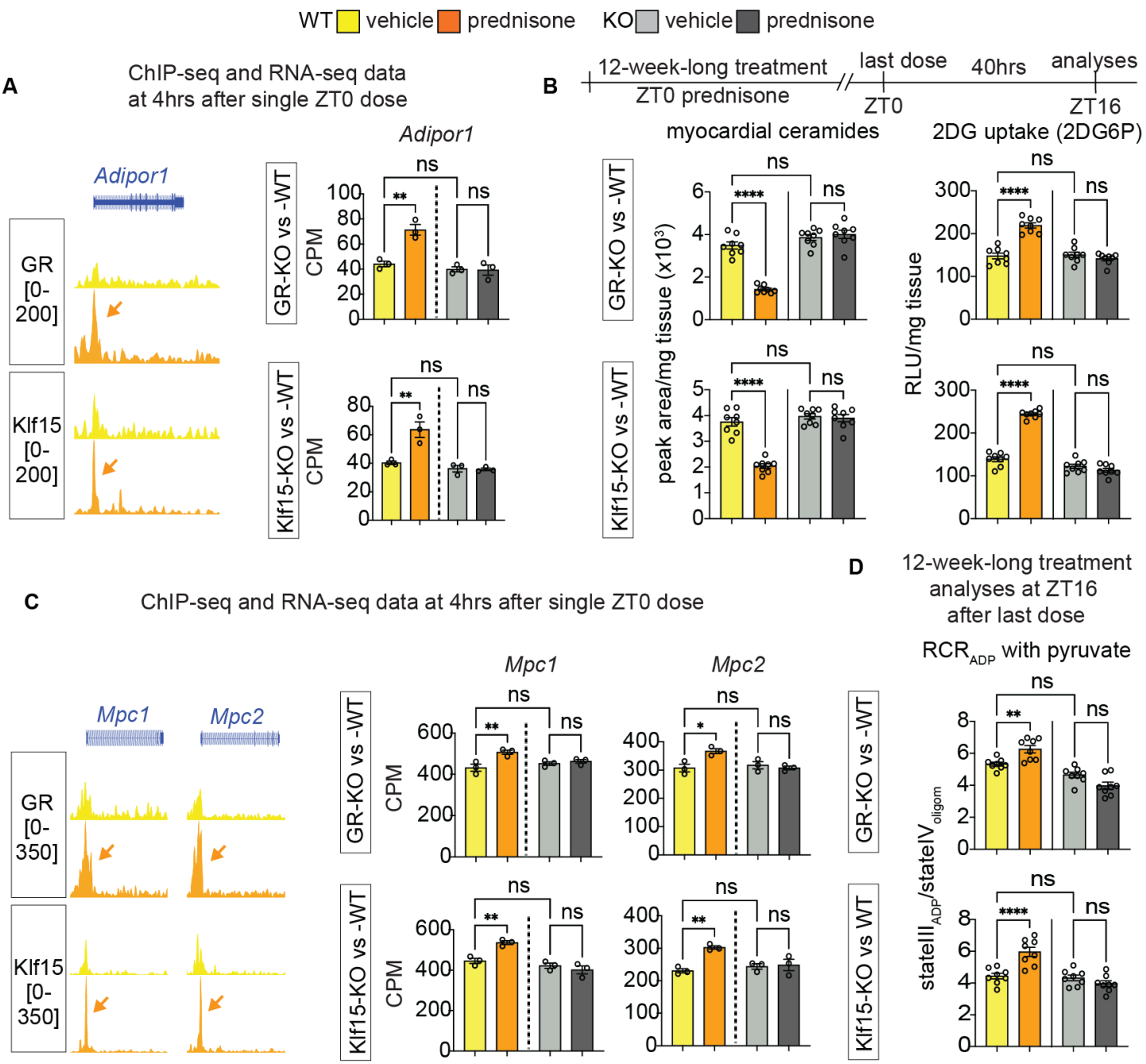

Figure 3. Cardiomyocyte GR and KLF15 are required for the ZT0 prednisone effects on gene transactivation, insulin sensitization and pyruvate oxidation in heart. (A) GR and KLF15 showed steroid-sensitive peaks on *Adipor1* TSS (arrows). Drug-induced upregulation was blunted by inducible cardiomyocyte-specific ablation of either GR or KLF15. **(B)** Transcriptional/metabolic effects of treatment appeared durable beyond the rest phase as GR and KLF15 were both required for the treatment effects on myocardial ceramide content reduction and insulin-stimulated glucose uptake increment in heart in the active phase (ZT16). **(C-D)** Similarly, GR and KLF15 were required for the drug effect on *Mpc1/2* transactivation, and for the chronic treatment effects on pyruvate oxidation in heart in the active phase. Shown are mean±S.E.M, histograms show also individual mouse values. n=3♂/group in A, C; n=8♂/group in B, D; 2w ANOVA + Sidak; *, P<0.05; **, P<0.01; ***, P<0.001; ****, P<0.0001.

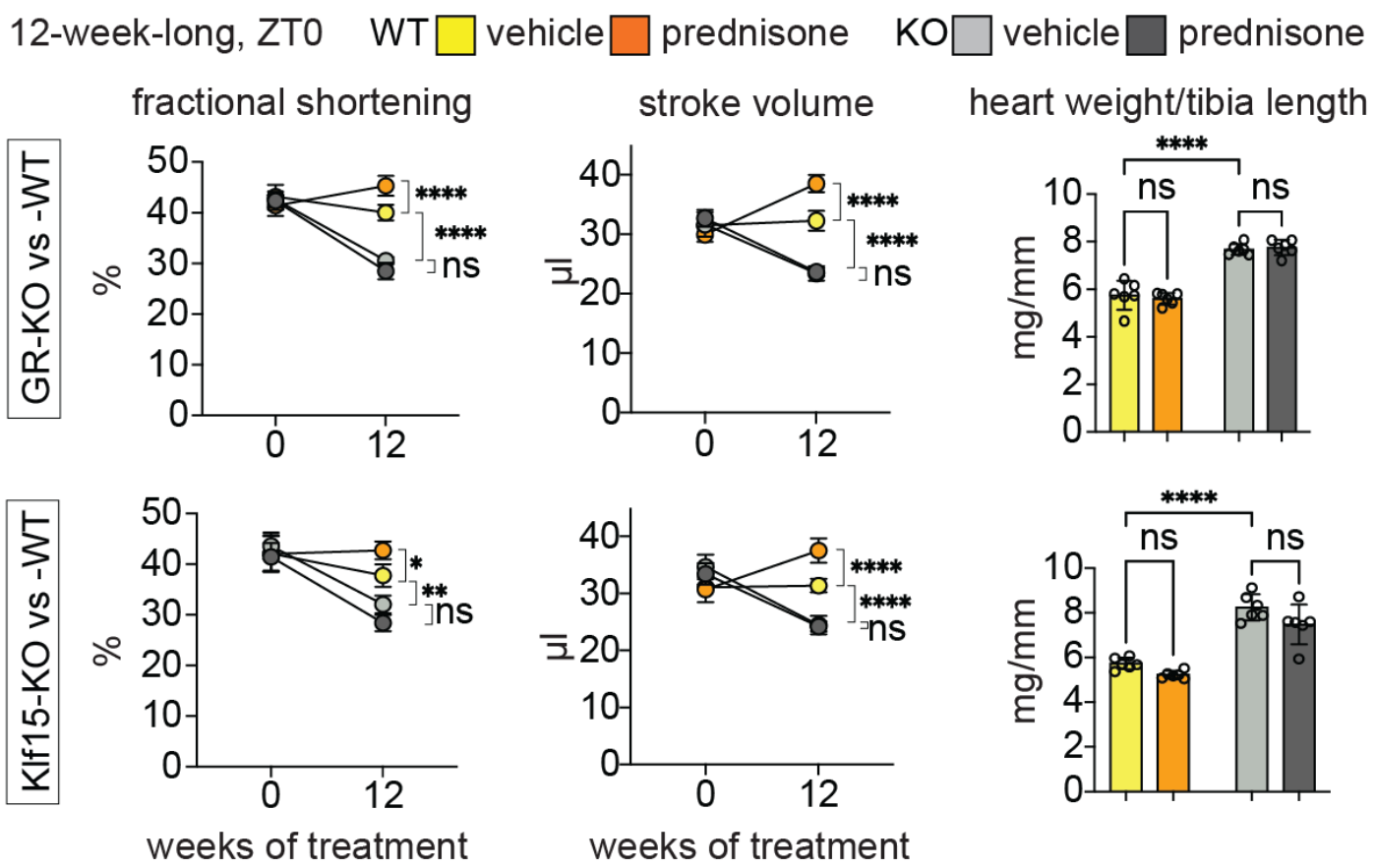

Figure 4. Functional cardiac assessments for chronic ZT0 prednisone effects on uninjured hearts after cardiomyocyte gene ablation. Either GR-KO or KLF15-KO induced significant losses in fractional shortening, stroke volume and gains in heart weight/tibia length compared to WT. In WT uninjured hearts, treatment increased stroke volume and fractional shortening, with no significant trends in heart weight. As expected, treatment had no sizable effects in KO hearts. Shown are mean±S.E.M, histograms show also individual mouse values. N=6♂/group; curves, 3w ANOVA + Sidak; histograms, 2w ANOVA + Sidak; *, P<0.05; **, P<0.01; ***, P<0.001; ****, P<0.0001.

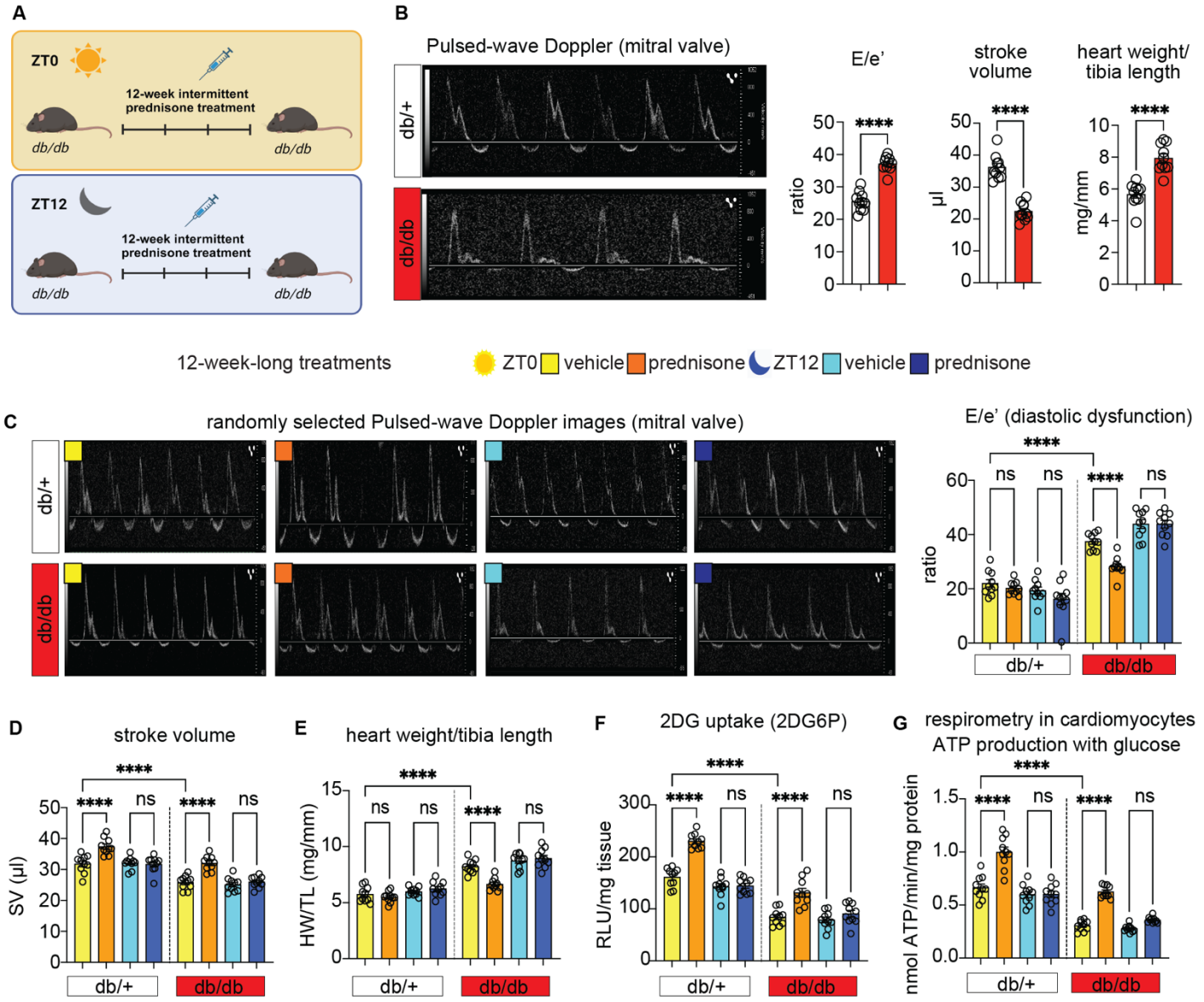

Figure 5. ZT0 glucocorticoid treatment rescues glucose oxidation and diastolic function in db/db mice. (A) Schematic showing the 12-week-long prednisone treatment of db/db and their littermate controls (db/+) at ZT0 and ZT12. **(B)** Representative images of pulse wave doppler echocardiography for mitral valve flow, and quantitation of baseline defects in E/e', stroke volume and heart mass in db/db mice. **(C)** ZT0 treatment decreased E/e' in db/db hearts to db/+-like levels, while ZT12 treatment had no sizable effects. **(D)** ZT0 but not ZT12 treatment increased stroke volume in both db/db and db/+ mice. **(E)** Cardiac hypertrophy was alleviated in db/db hearts by ZT0 but not ZT12 treatment. **(F)** Treatment increased glucose uptake in myocardial tissue, measured as 2DG uptake, in both db/+ and db/db hearts only with ZT0 dosing. **(G)** Treatment increased glucose-fueled ATP production calculated from Seahorse curves in isolated cardiomyocytes in both db/+ and db/db mice according to time of intake (ZT0 but not ZT12), increasing db/db values to control-like levels. Shown are mean±S.E.M, histograms show also individual mouse values. n=(5♀+5♂)/group; B, Welch's t-test; C-G, 3w ANOVA + Sidak; *, P<0.05; **, P<0.01; ***, P<0.001; ****, P<0.0001.

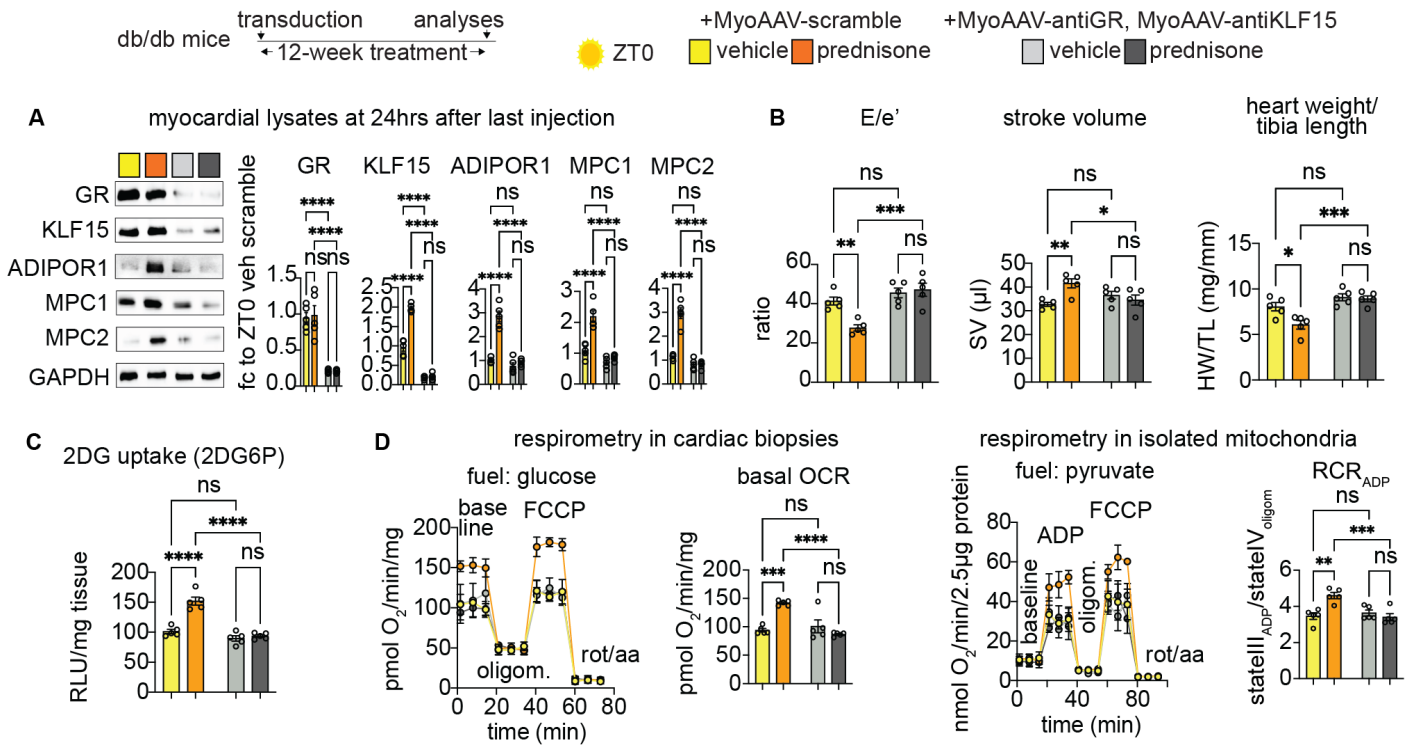

Figure 6. Knock-down of GR and KLF15 in db/db hearts in vivo blocks the ZT0 prednisone effects. (A) Representative WB showing knock-down of GR and KLF15 at 12-weeks after transduction and ZT0 prednisone regimen start, as well as blunting of the treatment effect on Adipor1, Mpc1 and Mpc2 protein level upregulation in hearts of db/db mice transduced with the knock-down vectors compared to mice transduced with scramble vectors. **(B-C)** Knock-down MyoAAV combination blocked the treatment effects on diastolic dysfunction (E/e'), stroke volume, cardiac hypertrophy (heart weight/tibia length) and insulin-driven glucose uptake (2DG6P). **(D)** Treatment increased glucose-fueled respiration (oxygen consumption rate, OCR) in permeabilized cardiac biopsies and pyruvate-fueled respiration (respiratory control ratio, RCR) in isolated myocardial mitochondria in scramble- but not knockdown-transduced hearts. Shown are mean±S.E.M, histograms show also individual mouse values. n=5 ♂/group; 2w ANOVA + Sidak; *, P<0.05; **, P<0.01; ***, P<0.001; ****, P<0.0001.

Supplementary Figures

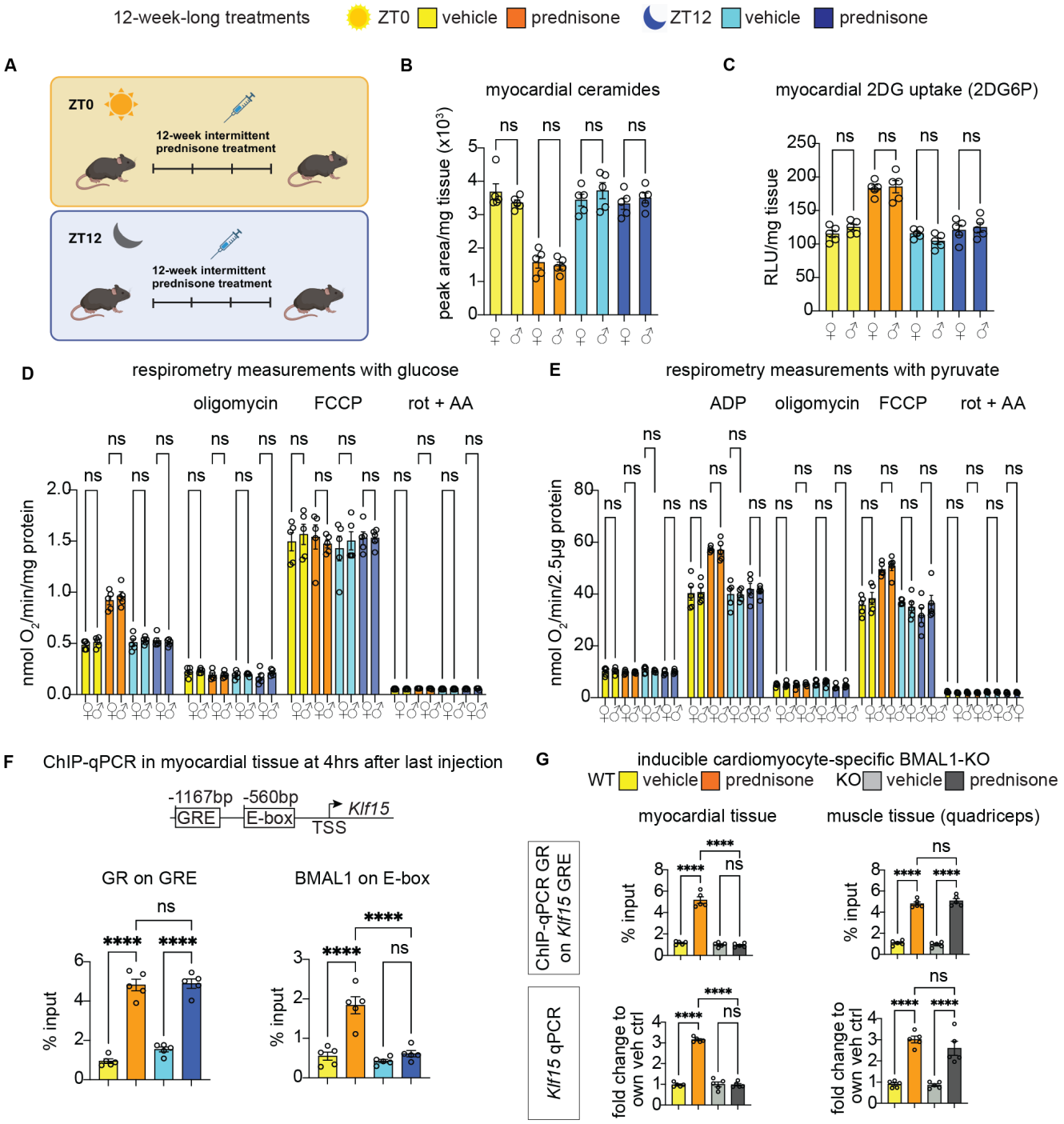

Supplementary Figure 1. Additional analyses related to Figure 1. (A) Graphical experimental design for wild-type mice. **(B)** Ceramide levels were decreased upon treatment with prednisone at ZT0, but not at ZT12. This effect was sex-independent. **(C)** Increased insulin-dependent 2DG uptake in heart showed no sexual dimorphism. **(D)** Although the cardiomyocytes showed an increase in basal glucose-fueled respiration ex vivo, no differences between the two sexes were observed. **(E)** ZT0 treatment increased ADP-stimulated respiration and respiratory control ratio with pyruvate. These effects were sex-independent. **(F)** While GR occupancy of *Klf15* promoter was increased by treatment independent from time-of-intake, ZT0 but not ZT12 treatment increased BMAL1 recruitment. **(G)** Ablation of BMAL1 in adult cardiomyocytes in vivo blocked the ZT0 prednisone-driven effects on GR occupancy of *Klf15* promoter and *Klf15* mRNA upregulation in heart (BMAL1 ablation) but not in muscle (no BMAL1 ablation). Shown are mean±S.E.M, histograms show also individual mouse values. n=(5♀+5♂)/group B-E, 5♂/group in F-G; 2w ANOVA+ Sidak; ns= non-significant. *, P<0.05; **, P<0.01; ***, P<0.001; ****, P<0.0001.

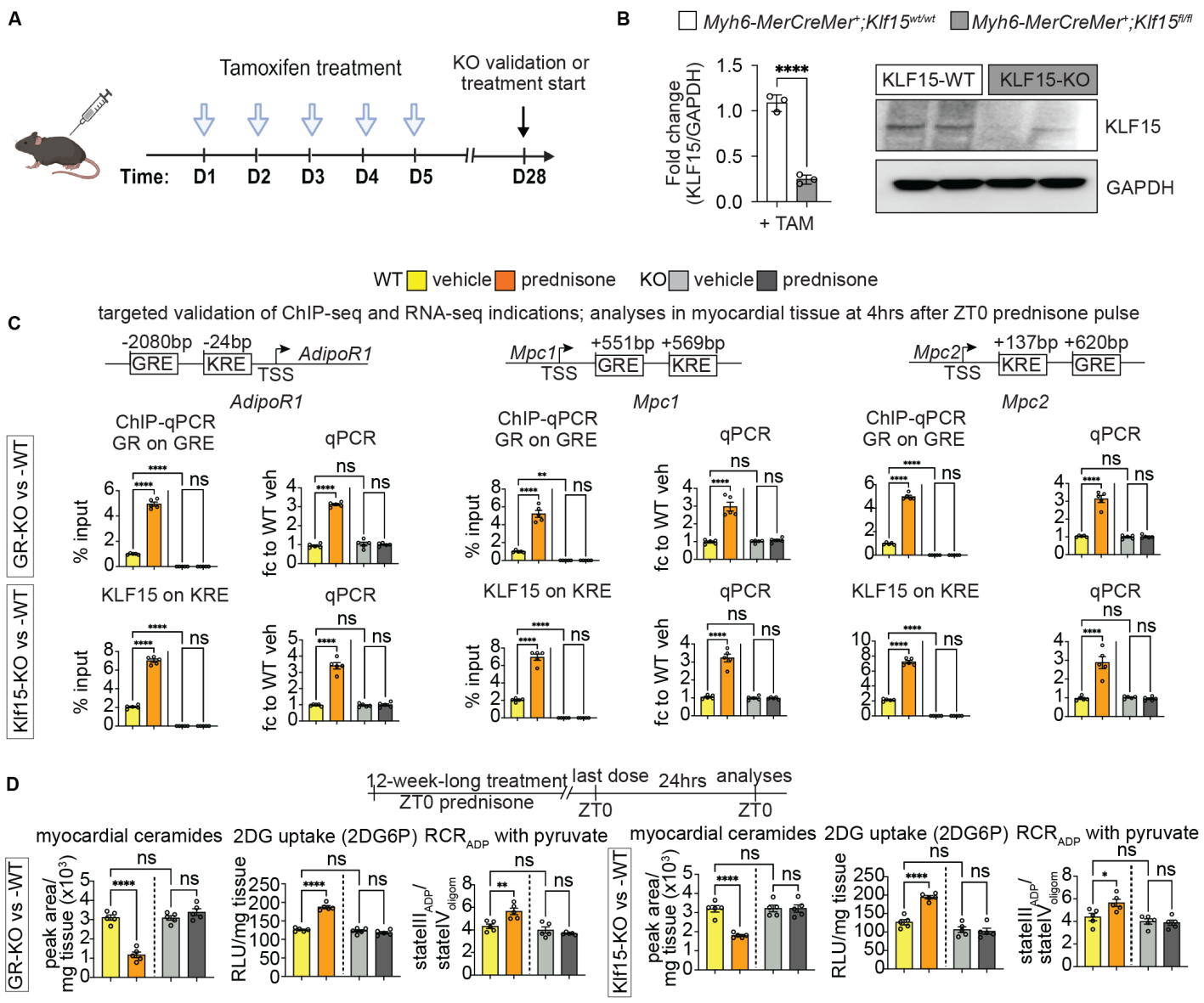

Supplementary Figure 2. Tamoxifen regimen, Klf15-KO validation and light-phase effects of chronic treatments in GR-KO and KLF15-KO hearts. (A) Schematic representing the generation and washout of tamoxifen-mediated inducible knockout mice for GR or KLF15. **(B)** Validation of KLF15 ablation in heart through WB. **(C)** Targeted validation through ChIP-qPCRs and qPCRs of ChIP-seq and RNA-seq indications of GR and KLF15 transactivation of *AdipoR1*, *Mpc1* and *Mpc2* in heart after ZT0 prednisone. **(D)** Related to Figure 3B-D. GR and KLF15 were both required for treatment effects on myocardial ceramides, glucose uptake and pyruvate oxidation at 24hrs from last ZT0 prednisone dose, i.e. in the rest phase. Shown are mean±S.E.M, histograms show also individual mouse values. B, n=3/group, Welch's t-test; C, n=5♂/group, 2w ANOVA + Sidak; *, P<0.05; **, P<0.01; ***, P<0.001; ****, P<0.0001.

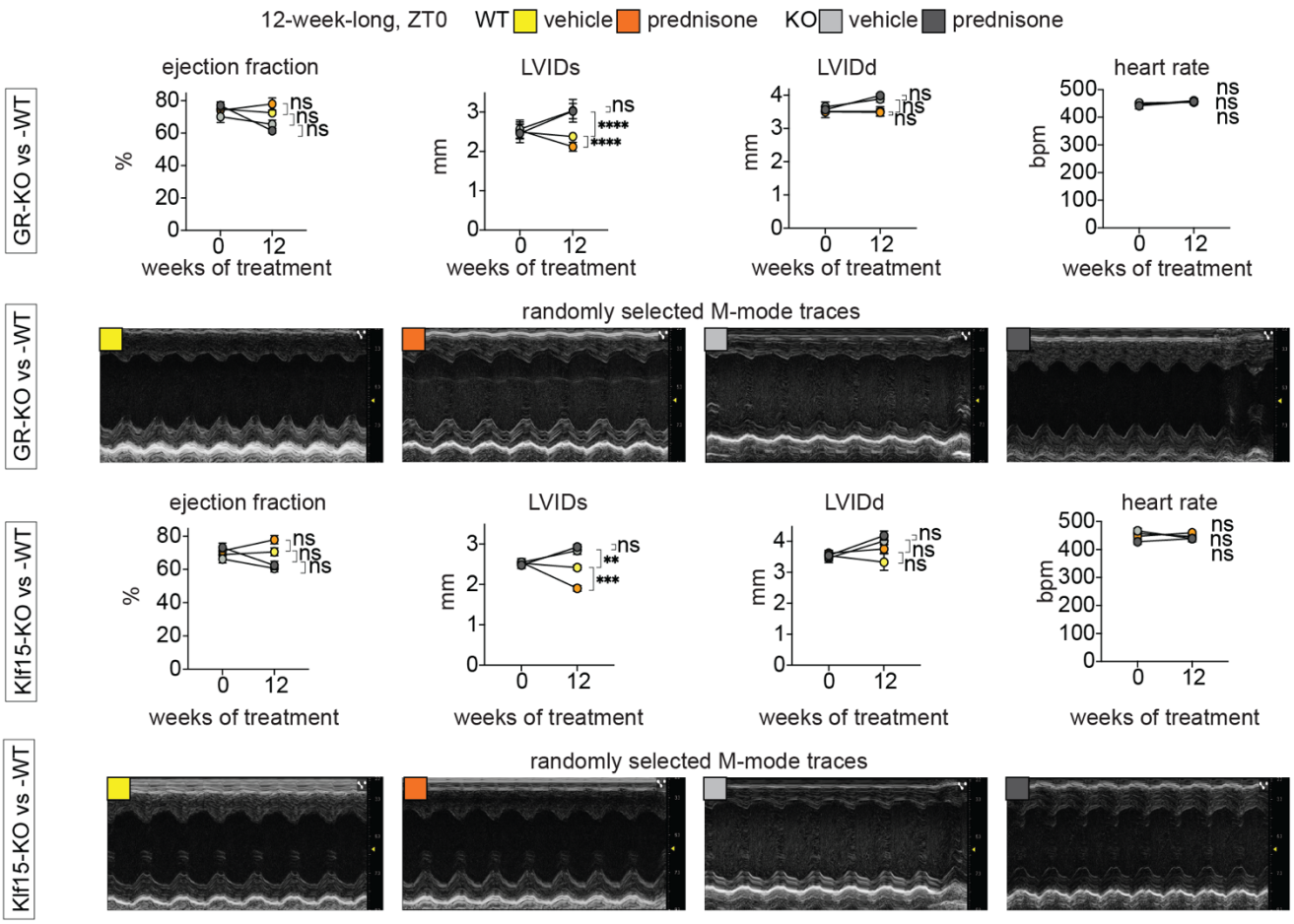

Supplementary Figure 3. Additional echocardiographic measurements related to Figure 4. In line with the trends in fractional shortening and strole volume (Figure 4), inducible ablation of either GR or KLF15 in cardiomyocytes enlarged the systolic left ventricle diameter (LVIDs) and induced non-significant declines in ejection fraction and gains in diastolic left ventricle diameter (LVIDd). In WT hearts, treatment induced a small significant reduction of LVIDs, a non-significant trend in increased ejection fraction and no appreciable changes in LVIDd. In KO hearts, treatment had no sizable effects. Heart rate during the echocardiographic measurements, i.e. under anesthesia, was not changed by either KO or treatment. Shown are mean±S.E.M, histograms show also individual mouse values. N=6♂/group; curves, 3w ANOVA + Sidak; histograms, 2w ANOVA + Sidak; *, P<0.05; **, P<0.01; ***, P<0.001; ****, P<0.0001.

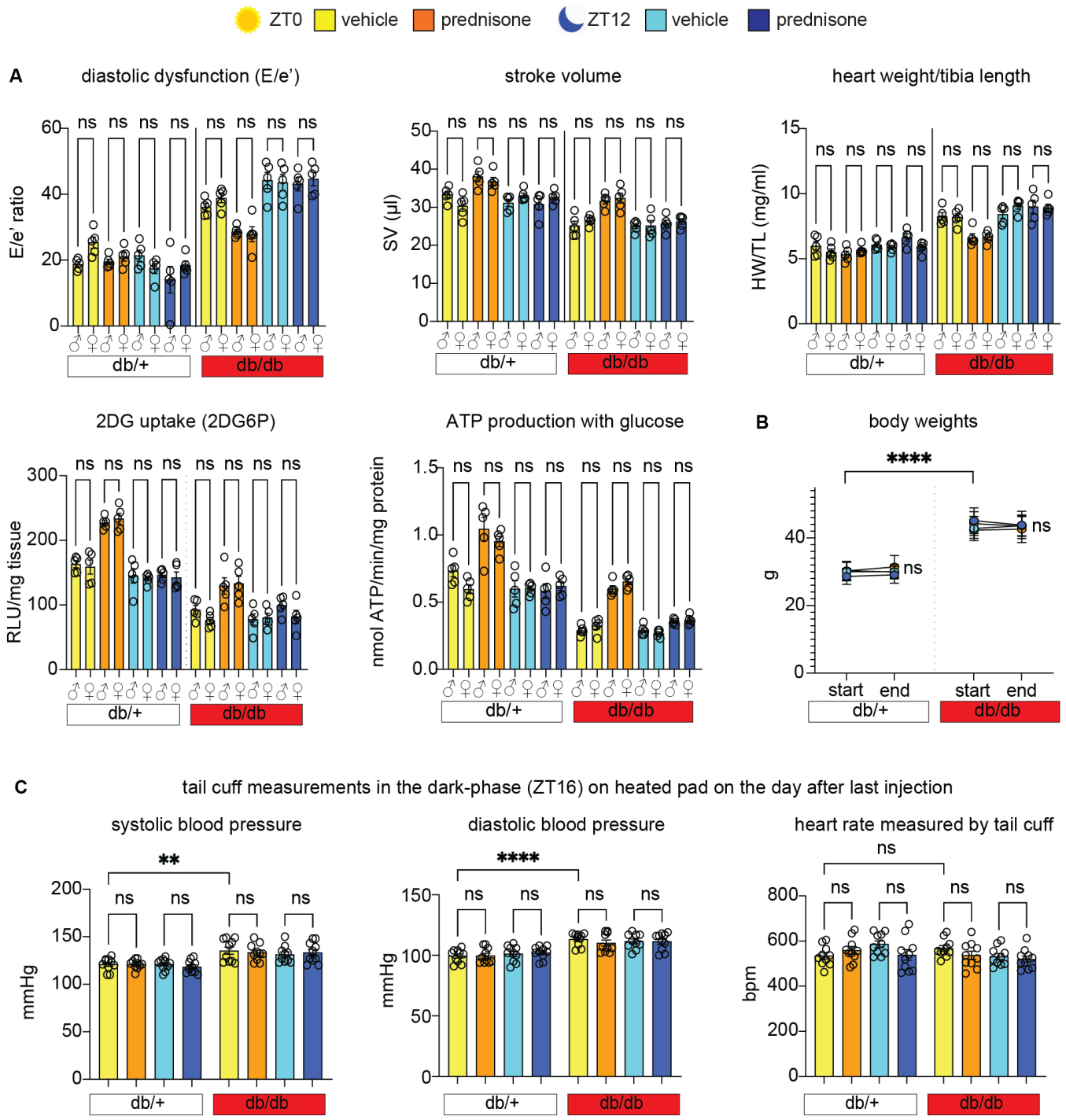

Supplementary Figure 4. Additional measurements of cardiac function and blood pressure related to Figure 5. (A) Sex-disaggregated measurements for male and female mice (db/+) and (db/db) for E/e', stroke volume, heart weight/tibia length, 2DG uptake and ATP-linked respiration in cardiomyocytes showed no sizable sexual dimorphism in the treatment effects, either with ZT0 or ZT12 prednisone. **(B)** Treatments had no sizable effects on body weight, which was significantly skewed by genotype. **(C)** Treatments had no sizable effects on blood pressure or heart rate during blood pressure measurements beyond the expected db/db-related mild hypertension in both systole and diastole. Shown are mean±S.E.M, histograms show also individual mouse values. n=(5♀+5♂)/group; 3w ANOVA + Sidak; *, P<0.05; **, P<0.01; ***, P<0.001; ****, P<0.0001.

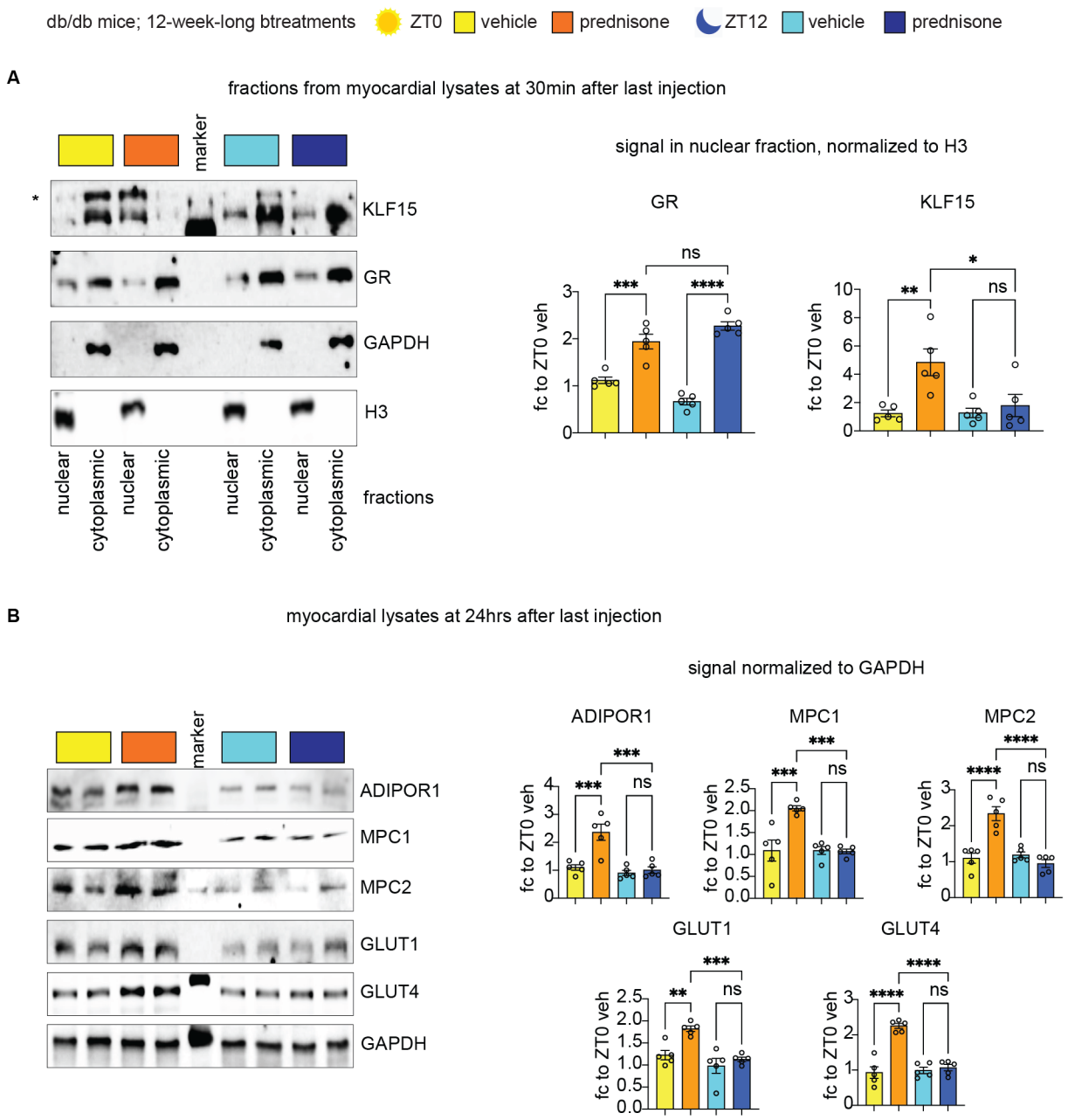

Supplementary Figure 5. Additional protein analyses in db/db hearts related to Figure 5. (A) WB in nuclear ($H3^+$) and cytoplasmic ($GAPDH^+$) fractions showed that time-of-intake changed treatment-driven nuclear translocation of KLF15 but not GR in db/db hearts. **(B)** ZT0 intermittent prednisone – but not ZT12 – increased the myocardial protein levels of Adipor1, Mpc1, Mpc2, Glut1 and Glut4 in db/db mice compared to vehicle. Shown are mean±S.E.M, histograms show also individual mouse values. n=5♂/group, 2w ANOVA + Sidak; *, P<0.05; **, P<0.01; ***, P<0.001; ****, P<0.0001.

503 **METHODS AND MATERIALS**

504 **Sex as biological variable**

505 We performed the bulk of our wild-type and diabetic mice experiments in both males and females, analyzing and
506 reporting the physiological, molecular and histological assessments as sex-aggregated in main figures and sex-
507 disaggregated in the supplementary figures. We did not find sizable sex-specific patterns. Therefore, we
508 performed our unbiased omics-based screenings and subsequent KO- or knockdown-based proofs of
509 requirement only in male mice to minimize variability and overall mouse number used.

510

511 **Animal handling and treatments**

512 Mice were housed in a pathogen-free facility in accordance with the American Veterinary Medical Association
513 (AVMA) and under protocols fully approved by the Institutional Animal Care and Use Committee (IACUC) at the
514 Cincinnati Children's Hospital Medical Center (#2023-0002). Consistent with the ethical approvals, all efforts
515 were made to minimize suffering. Euthanasia was performed through carbon dioxide inhalation followed by
516 cervical dislocation and heart removal.

517

518 Mice were maintained on a 12h/12h light/dark cycle, and diet/pharmacological treatments were initiated at ~ 12
519 weeks of age. Mice were obtained and interbred from the Jakson Laboratories (Bar Harbor, ME; JAX strain
520 number listed) or from collaborators: WT C57BL/6 mice #000664, *Myh6-MerCreMer* mice #005657, *GR-flox* mice
521 #021021, *Arntl-flox* (BMAL1-flox) #007668, *Klf15-flox* mice #029787 (provided by Dr. Jain, Brown U), db/db
522 #000642; Klf15-3xFLAG mice (25) were provided by Dr. Haldar (Amgen & UCSF). Gene ablation was induced
523 with tamoxifen at ~8 weeks of age i.p. tamoxifen (20 mg/kg/day for 5 days; Sigma #T5648) and analyses were
524 performed after 4 weeks of tamoxifen washout, i.e. at ~16 weeks of age.

525

526 Weekly prednisone treatment consisted of once-weekly intraperitoneal injection of prednisone (1 mg/kg; #P6254,
527 Sigma-Aldrich, St. Louis, MO). The injectable solution was diluted from a stock (5 mg/ml) in dimethyl sulfoxide
528 (DMSO; #D2650, Sigma-Aldrich, St. Louis, MO) in a 50-µl volume. Injections were conducted either at the
529 beginning of the light phase (ZT0; lights on) or at the beginning of the dark phase (ZT12; lights off). Tissues were

530 harvested at 4 hours post-injection for epigenetic/transcriptional assays and at 24 hours post-injection for
531 metabolic/physiologic assays. All in vivo, ex vivo, and postmortem analyses were conducted blinded to treatment
532 group.
533
534 For systemic AAV experiments, 6-month-old db/db mice were administered to either vehicle or 12-week long
535 prednisone regimen at the beginning of the light phase (ZT0; lights on). These mice were further injected retro-
536 orbitally with either $6x10^{12}$ genome copies/injection MyoAAV-scrambleshRNA or $1x10^{12}$ genome copies/injection
537 for each of the MyoAAV-*Nr3c1*shRNA and MyoAAV-*Klf15*shRNA vectors (Vector Builder cargo vectors #
538 VB010000-0023jze, VB240517-1300eyt, VB240517-1305cxu, VB240517-1306ywz, VB900144-1448eer,
539 VB240517-1307ced, VB240517-1308zdv; anti-*Nr3c1* shRNA sequences: AGGATTGCAAGCCTCTTATTT,
540 TGAGATTCGAATGACTTATAT, TTTGCTCCTGATCTGATTATT; anti-*Klf15* shRNA sequences:
541 CATTTCTGCTTCCCTGAATTT, CTACCCTGGAGGAGATTGAAG, ACCGAAATGCTCAGTGGGTTA; U6
542 promoter for all scramble and shRNA constructs) while under inhaled isoflurane anesthesia. All MyoAAV
543 injections were diluted in sterile PBS. To prepare and isolate AAV virions, we followed the procedures we
544 previously reported (50).
545
546 **RNA-seq and qPCR analyses**
547 RNA-seq was conducted on RNA extracted from left ventricle myocardial tissue. Each heart was immediately
548 snap frozen in 1ml TRIsure (Bioline, BIO-38033) using liquid nitrogen. RNAs from each heart were re-purified
549 using RNeasy Mini Kit (Cat #74104; Qiagen, Germantown, MD). RNA-seq was performed at the DNA Core
550 (CCHMC). 150 ng – 300 ng of total RNA determined by Qubit (Cat #Q33238; Invitrogen, Waltham, MA) high-
551 sensitivity spectrofluorometric measurement was poly-A selected and reverse transcribed using Illumina's
552 TruSeq stranded mRNA library preparation kit (Cat# 20020595; Illumina, San Diego, CA). Each sample was
553 fitted with one of 96 adapters containing a different 8 base molecular barcode for high level multiplexing. After
554 15 cycles of PCR amplification, completed libraries were sequenced on an Illumina NovaSeqTM 6000,
555 generating 20 million or more high quality 100 base long paired end reads per sample. A quality control check
556 on the fastq files was performed using FastQC. Upon passing basic quality metrics, the reads were trimmed to
557 remove adapters and low-quality reads using default parameters in Trimmomatic [Version 0.33]. In the next step,

558 transcript/gene abundance was determined using kallisto [Version 0.43.1]. The trimmed reads were then mapped
559 to mm10 reference genome using default parameters with strandness (R for single-end and RF for paired-end)
560 option in Hisat2 [Version 2.0.5]. In the next step, transcript/gene abundance was determined using kallisto
561 [Version 0.43.1]. We first created a transcriptome index in kallisto using Ensembl cDNA sequences for the
562 reference genome. This index was then used to quantify transcript abundance in raw counts and counts per
563 million (CPM). Differential expression (DE genes, FDR<0.05) was quantitated through DESeq2. PCA was
564 conducted using ClustVis. Gene ontology pathway enrichment was conducted using the Gene Ontology analysis
565 tool.
566
567 Total RNA was extracted from cryo-pulverized liver tissue and hiPSC-derived hepatocyte-like cells using Trizol
568 (Thermo Fisher Scientific) and 1 ug RNA was reverse-transcribed using SuperScript™ IV VILO™ Master Mix
569 (#11756050, Thermo Fisher Scientific). RT-qPCRs were conducted in three replicates using 1X SYBR Green
570 Fast qPCR machine (Bio-Rad, Hercules, CA; thermal profile: 95C, 15 sec; 60C, 30sec; 40x; melting curve). The
571 2-ΔΔCT method was used to calculate relative gene expression. GAPDH was used as the internal control.
572 Primers were selected among validated primer sets from MGH PrimerBank as follows (Gene, Forward, Reverse):
573 *Klf15,* GAGACCTTCTCGTCACCGAAA*,* GCTGGAGACATCGCTGTCAT*; Adipor1,*
574 TCTTCGGGATGTTCTTCCTGG*,* TTTGGAAAAAGTCCGAGAGACC*; Mpc1,*
575 CTCCAGAGATTATCAGTGGGCG*,* GAGCTACTTCGTTTGTTACATGGC*; Mpc2,*
576 CTCAGTCCACTGTGTTGATGGC*,* ATCCGAAACAGCTGAGAGGCTC.
577
578 **Mass-spec analysis of ceramides in myocardial tissue**
579 Untargeted lipidomics was performed on myocardial tissue from mice treated for 12-week-long intermittent
580 treatments with vehicle or weekly prednisone. Whole hearts were snap-frozen and then ground to powder with
581 dry ice-chilled mortar and pestle. Frozen samples were sent on dry ice to mass spectrometry Core at the
582 Cincinnati Children's Hospital Medical Center, where LC-MS and data analysis were performed. Briefly 10 µl
583 sample was added to 30 µl of internal standard, except for the blank calibrator. Then 300 µl of Butanol/Methanol
584 (3:1) was added to sample aliquot tube and vortexed for 10 mins. Next, 150 µl of Heptane/Ethyl Acetate (3:1)
585 was added to the sample tube and vortexed for 5 mins. The contents of the sample aliquot were then transferred

586 to a large glass tube, to which 150 µl of Heptane/Ethyle Acetate was added and vortexed for 5 mins. Then, 300
587 ul of 1% Acetic acid was added to the original tube to wash, vortexed for 5 mins and then added back to the
588 glass tube. The glass tube was further vortexed for 5 mins and let sit for 5 mins. The upper organic phase of ~
589 200 µl was transferred to a new glass tube. To this, 320 µl Heptane/Ethyl Acetate (3:1) was added to the water
590 phase, vortexed for 5 mins and let sit for 5 mins. Next, 280 µl of upper organic phase (second extract) was
591 transferred to the first extract. This step is repeated once. The upper organic phase (third extract) of 100 µl was
592 combined with other extracts and dried down with nitrogen in a heating block set to 40°C. The resuspended lipid
593 extracts (2 µl) were loaded and separated through Xevo QTOF G2-S mass spectrometer (Waters Corp). All
594 calculations were performed using QuanLynx.

595 **Chromatin immunoprecipitation and sequencing**

596 Whole hearts were cryopowdered using a liquid nitrogen cooled RETSCH Cryomill. The cryopowdered tissue
597 was then fixed in 10 ml of 1% paraformaldehyde (PFA) for 30 min at room temperature with gentle nutation.
598 Fixation was quenched 1 ml of 1.375 M glycine (Cat# BP381-5, Thermo Fisher Scientific, Waltham, MA) with
599 gentle nutation for 5 mins at room temperature. After centrifugation at 3,000*g* for 5 mins at 4°C, the pellet was
600 resuspended in cell lysis buffer as per reported conditions, supplementing the cell lysis buffer with cytochalasin
601 B (3 µg/ml) and rotating for 10 min at 4°C. Nuclei were pelleted at 300*g* for 10 mins at 4°C and subsequently
602 processed following the reported protocol with the adjustment of adding cytochalasin B (3 µg/ml) into all solutions
603 for chromatin preparation and sonication, antibody incubation, and wash steps. Chromatin was then sonicated
604 for 15 cycles (30 s, high powder, 30-s pause, and 500-µl volume) in a water bath sonicator set at 4°C (Bioruptor
605 300. Diagenode, Denville, NJ). After centrifuging at 10,000*g* for 10 mins at 4°C, sheared chromatin was checked
606 on agarose gel for a shear band comprised between ~150 and ~600 bp. Two micrograms of chromatin were kept
607 for pooled input controls, whereas ~50 µg of chromatin was used for each pull-down reaction in a final volume
608 of 2 ml rotating at 4°C overnight. Primary antibodies were as follows: rabbit poly-clonal anti-GR (#A2164,
609 ABclonal), mouse monoclonal ANTI-FLAG M2 (#F1804, Sigma-Aldrich, St. Louis, MO). Chromatin complexes
610 were precipitated with 100 µl of Dynabeads M-280 (Sheep anti-mouse, # 11202D; sheep anti-rabbit, #11204;
611 Thermo Fisher Scientific, Waltham, MA). After washes and elution, samples were treated with proteinase K (Cat#
612 19131, QIAGEN, Hilden, Germany) at 55°C, and cross-linking was reversed through overnight incubation at

613 65°C. DNA was purified using a MinElute purification kit (Cat# 28004, QIAGEN, Hilden, Germany) and
614 quantitated using Qubit reader and reagents. Library preparation and sequencing were conducted at the CCHMC
615 DNA Core, using TruSeq ChIP-seq library prep (with size exclusion) on ~10 ng of chromatin per ChIP sample or
616 pooled inputs and HiSeq 50-bp was conducted using HOMER software (v4.10) after aligning fastq files to the
617 mm10 mouse genome using bowtie2. PCA was conducted using ClustVis. Heatmaps of peak density were
618 imaged with TreeView3. Peak tracks were imaged through WashU epigenome browser. Gene ontology pathway
619 enrichment was conducted using the gene ontology analysis tool.
620 For ChIP-qPCR analyses, muscle chromatin was immunoprecipitated following the conditions for ChIP-seq.
621 Input and IP chromatins were diluted 100X and assayed using the qPCR conditions. The regions identified in the
622 Klf15 promoter were a GRE at -1167bp from TSS (primers, Fw TCTAGACAGCTGGGGCATCT, Rev
623 GACAGACCTTCCTTCCTGGC) and a BMAL1 E-Box at -560bp from TSS (primers, Fw
624 AAGCACAGACTCCTTCCGTG, Rev CGCTACCCTAGACTTCTGCG). Additional regions and primers: *Adipor1*
625 GRE, Fw agctggggttctaggacact, Rev gctgctccccctttaagtgt; *Adipor1* KRE, Fw aagattgccttcccagctcc, Rev
626 ggaggggccggaaatgttta; *Mpc1* GRE, Fw gctcttggttaaggcgacct, Rev acacatgattgtccggtccc; *Mpc1* KRE, Fw
627 gctcttggttaaggcgacct, Rev acacatgattgtccggtccc; *Mpc2* KRE, Fw atagcgagatccaagccagc, Rev
628 ctagggatcgacagcagcag; *Mpc2* GRE, Fw ctgctgctgtcgatccctag, Rev gctgagaccagacagacacc.Signal in IP
629 chromatin was quantitated as % of input signal per qPCR calculations.

630 **2-DG-6-phosphatase assay**

631 For measuring the uptake of 2-DG-6-phosphatase, Glucose uptake-Glo™ assay (Cat# J1341, Promega) was
632 utilized to inject 1mM 2DG into mice for 30 mins before euthanasia. After 30 mins, the whole heart tissues were
633 harvested and stored at -80C until ready to use. Next, the reagents from the kit were combined for reaction
634 mixtures according to manufacturer's instructions and incubated at room temperature for 1 hr. The frozen heart
635 tissues were crushed into a fine powder and 20 - 50 mg of tissue powder was used for the assay. After 1 hour
636 incubation of reaction mixture, 25 µl of Neutralization buffer was added to reaction mixture. Next, 125 µl of
637 reaction mixture and neutralization buffer was added to powdered heart tissue and incubated for 1 hr. After
638 incubation, the samples were centrifuged for 5 mins at 10,000*g* and 125 µl of the supernatant was loaded onto
639 a 96-well plate for luminescence readings.

640 **Respirometry on cardiac biopsies, cardiomyocytes and isolated mitochondria**

641 For cardiac biopsies, whole hearts were harvested and multiple transverse cuts were performed with a scapel in
642 the left ventricular region with small scissors. Size matched tissue biopsies were prepared as thin as possible
643 (~0.5mm^2) cover the bottom of the seahorse plate's well. The biopsies were permeabilized in 100ug/ml saponin
644 solution (Sigma #SAE0073) and incubated in XF base medium with 10 mM glucose, 2 mM L-glutamine, and 1
645 mM pyruvate (Sigma #G7021, #G7513, #P2256) in 37°C non-CO_2 incubator for 30 mins. Regular seahorse
646 protocol is followed with basal reads and injections of oligomycin, FCCP, Rotenone/Antimycin following reported
647 conditions. Basal OCR was calculated as baseline value (average of 3 consecutive reads) minus value after
648 rotenone/antimycin addition (average of 3 consecutive reads). Basal OCR values were normalized to total protein
649 content using Bradford assay.

650 For cardiomyocytes, respirometry was performed on freshly isolated cells. Cardiomyocytes are isolated adapting
651 to previously reported conditions. In anesthetized mice, the descending aorta is cut, and the heart is immediately
652 flushed by injecting 7ml pre-warmed EDTA buffer into the right ventricle. Immediately afterwards, the ascending
653 aorta is clamped using Reynolds forceps, the heart is removed and kept in the 60 mm dish with pre-warmed
654 EDTA buffer. The digestion process is proceeded by injecting 10 ml pre-warmed EDTA buffer to the apex of left
655 ventricle. The heart is then transferred to the 60 mm dish with perfusion buffer and 3 ml perfusion buffer is
656 injected to flush out the EDTA buffer. Then the heart is transferred to another 60 mm dish with pre-warmed
657 180U/ml Collagenase II buffer and 30-40 ml collagenase buffer is injected into the apex of LV. Then the heart is
658 cut from the clamp, the ventricular myocardial tissue is pulled gently into small pieces using forceps and further
659 dissociated by gentle pipetting. The cardiomyocyte suspension is passed through a 200 μm mesh, and the
660 digestion is stopped by adding 5ml of stop buffer. Cardiomyocytes are then centrifuged at 100*g* for 3 mins,
661 resuspended in the stop buffer with increasing concentration of calcium (100 μM, 400 μM, and 1000 μM), re-
662 centrifuged and then plated in laminin-coated Seahorse plates in culture media. After 1 h incubation, the culture
663 media is aspirated and Seahorse media is added for respirometry, which starts after an additional 1 h equilibrium
664 in a CO_2-free incubator. Buffer compositions: EDTA buffer contains 130 mM NaCl, 5mM KCl, 0.5mM NaH_2PO_4,
665 10mM HEPES, 10mM glucose, 10mM BDM, 10mM Taurine, 5 mM EDTA, pH 7.8; Perfusion buffer contains
666 130 mM NaCl, 5 mM KCl, 0.5 mM NaH_2PO_4, 10 mM HEPES, 10 mM glucose, 10 mM BDM, 10 mM taurine,
667 1 mM $MgCl_2$, pH 7.8; Collagenase buffer contains 220U/ml Collagenase II; Stop buffer consists of Perfusion

668 buffer supplemented with 5% sterile fetal bovine serum; Culture medium (250 mL) contains 2.45g Hanks' salt,
669 5 mL non-essential amino acids, 2.5 mL MEM Vitamin Solution, 0.0875g $NaHCO_3$, 2.5 mL PenStrep 10X,
670 1 mg/mL bovine serum albumin. Regular seahorse protocol is followed with basal reads and injection
671 of oligomycin, FCCP, Rotenone/Antimycin following reported conditions. Basal OCR was calculated as baseline
672 value (average of 3 consecutive reads) minus value after rotenone/antimycin addition (average of 3 consecutive
673 reads). Basal OCR values were normalized to total protein content, assayed in each well after the Seahorse ran
674 through homogenization and Bradford assay.
675 Mitochondrial ATP production rate was calculated as $OCR_{ATP} * 2$ (mol O in mol O_2) $*$ 2.75 (Seahorse P/O), where
676 OCR_{ATP} is the difference between baseline and oligomycin OCR. Nutrients: 10 mM glucose or 10 mM pyruvate;
677 inhibitors: 0.5 μM rotenone + 0.5 μM antimycin A (Agilent). Respiratory control ratio (RCR) values were obtained
678 from isolated mitochondria from myocardial tissue. Tissues from the left ventricle are harvested from the mouse
679 and cut up into very fine pieces. The minced tissue is placed in a 15 mL conical tube (USA Scientific #188261)
680 and 5 mL of MS-EGTA buffer with 1 mg Trypsin (Sigma #T1426-50 MG) is added to the tube. The tube is quickly
681 vortexed, and the tissue is left submerged in the solution. After 2 min, 5 mL of MS-EGTA buffer with 0.2% BSA
682 (Goldbio #A-421-250) is added to the tube to stop the trypsin reaction. MS-EGTA buffer: Mannitol (#M0214-45,
683 ChemProducts), Sucrose (#100892, Millipore), HEPES (#15630–080, Gibco), EGTA (#E14100–50.0, RPI). The
684 tube is inverted several times to mix then set to rest. Once the tissue has settled to the bottom of the tube, 3 mL
685 of buffer is aspirated, and the remaining solution and tissue is transferred to a 10 mL glass tissue homogenizer
686 (Avantor # 89,026–382). Once sufficiently homogenized the solution is transferred back into the 15 mL conical
687 tube and spun in the centrifuge at 1,000g for 5 min at 4 °C. After spinning, the supernatant is transferred to a
688 new 15 mL conical tube. The supernatant in the new tube is then centrifuged at 12,000g for 10 min at 4 °C to
689 pellet the mitochondria. The supernatant is discarded from the pellet and the pellet is then resuspended in 7 mL
690 of MS-EGTA buffer and centrifuged again at 12,000g for 10 min at 4 °C. After spinning, the supernatant is
691 discarded, and the mitochondria are resuspended in 1 mL of Seahorse medium (Agilent #103335–100) with
692 supplemented 5 mM pyruvate (Sigma #P2256-100G). After protein quantitation using a Bradford assay (Bio-Rad
693 #5000001), 2.5 μg mitochondria are dispensed per well in 180 μl total volumes and let to equilibrate for 1 h at 37
694 degrees C. 20 μl of 5 mM ADP (Sigma #01905), 50 μM Oligomycin (Milipore #495455-10 MG), 100 μM Carbonyl
695 cyanide-p-trifluoromethoxyphenylhydrazone (TCI #C3463), and 5 μM Rotenone (Milipore #557368-

696 1 GM)/Antimycin A (Sigma #A674-50 MG) are added to drug ports A, B, and C, respectively. At baseline and
697 after each drug injection, samples are read three consecutive times. RCR was calculated as the ratio between
698 state III (OCR after ADP addition) and uncoupled state IV (OCR after oligomycin addition). All Seahorse
699 measurements were conducted blinded to treatment groups.
700
701 **Western blotting**
702 Protein analyses in liver were performed on ~ 50 ug total lysates from the whole heart. Cyro-pulverized liver
703 tissue was incubated in RIPA buffer (Cat #89900, Thermo Fisher Scientific, Waltham, MA) supplemented with 1x
704 protease/phosphatase inhibitor (Cat #78440, Thermo Fisher Scientific, Waltham, MA) for 30 mins and sonicated
705 for 10 secs twice. The samples were then centrifuged at 10,000 rpm for 10 mins at 4°C. Supernatant containing
706 the protein is transferred into a new tube and used as a total lysate. For total cell lysates from culture cells, cells
707 were harvested and resuspended in RIPA buffer containing 1x protease and phosphatase inhibitors. Lysates
708 were incubated for 30 mins and centrifuged at 10,000 rpm for 10 mins at 4°C. The supernatant was used as a
709 total cell lysate. The protein concentrations of the supernatants were determined using the Pierce BCA Protein
710 Assay kit (Cat #23227, Thermo Fisher Scientific, Waltham, MA). Equal amounts of protein were separated using
711 SDS-PAGE and transferred to a PVDF membrane (Cat #1620174, BioRad, Hercules, CA). Membranes were
712 blocked in 5% milk in TBST for 1 hour at room temperature and then incubated overnight at 4°C with primary
713 antibodies: Mouse Klf15 monoclonal antibody (Cat# sc-271675, Santa Cruz Biotechnology), Rabbit Gapdh
714 monoclonal antibody (Cat# A10868, AC001 ABclonal), Rabbit Histone H3 polyclonal antibody (Cat# A2348,
715 ABclonal), Mouse GR monoclonal antibody (Cat# sc-393232, Santa Cruz Biotechnology), Rabbit AdipoR1
716 polyclonal antibody (Cat# A16527, ABclonal), Rabbit Mpc1 polyclonal antibody (Cat# A20195, ABclonal), Rabbit
717 Mpc2 polyclonal antibody (Cat# A20196, ABclonal), Rabbit Glut1 polyclonal antibody (Cat# A11208, ABclonal),
718 Rabbit Glut4 polyclonal antibody (Cat# A7637, ABclonal) followed by incubation with HRP-conjugated secondary
719 antibodies: Peroxidase AffiniPure Goat Anti-Rabbit IgG (H+L) (Cat# 111-035-003, Jackson ImmunoResearch
720 Labs, West Grove, PA) for 1 hour at room temperature. Immunoreactive bands were visualized by
721 chemiluminescence using Pierce Enhanced Chemiluminescent western blotting substrate (Cat #32106, Thermo
722 Fisher Scientific, Waltham, MA).
723

724 **Nuclear and cytoplasmic fraction analysis**

725 The separation of nuclear and cytoplasmic protein analysis was performed using NE-PER nuclear and
726 cytoplasmic extraction kit (Invitrogen #78835). Briefly, 100 mg of the heart tissues were homogenized, and 1 ml
727 of CERI solution was added and vortexed vigorously on high setting for 15 sec. Following incubation on ice for
728 10 mins, 55 µl od ice-cold CERII solution was added, vortexed, and incubated for 1 minute and centrifuged at
729 16,000g for 5 mins. The supernatant containing cytoplasmic fraction was separated and collected into a new 1.5
730 ml Eppendorf tube. The insoluble is suspended in 500 µl of ice-cold NER solution. The sample was then placed
731 on ice for 40 mins and vortexed every 10 mins for 1 sec. Finally, the samples were centrifuged at 16,000g for 10
732 mins. The supernatant containing the nuclear fraction was separated into a new 1.5 ml Eppendorf tube. All
733 samples were stored at -80°C until use. The protein concentration was determined by Bio-Rad protein assay as
734 described previously. Once the protein concentration was determined, western blotting analysis was carried out
735 as previously described.

736 **Measurement of Blood pressure by Tail-cuff Plethysmography**

737 The CODA 8 system (Kent Scientific, Torrington, CT) was used to noninvasively measure blood pressure in mice
738 through tail-cuff recordings. It was factory calibrated, and standard settings and procedures were adhered to as
739 recommended by the manufacturer. Before beginning the experiments, the occlusion and VPR cuffs were
740 routinely checked. Experiments were carried out in a controlled environment maintained at 22 ± 2°C, where mice
741 were acclimated for an hour prior to measurements. Mice were gently guided into the restraint tubes and tube
742 end holders were adjusted at the tail's base, with the VPR sensor cuff positioned next to it. Heating pads provided
743 with the CODA 8 system were preheated to 33-35°C. Mice were warmed on these pads for 5 mins before and
744 during the blood pressure recording. To obtain blood pressure readings, the occlusion cuff was inflated to 25 mm
745 Hg and then deflated over 20 seconds. The VPR sensor cuff detected the changes in tail volume as blood flow
746 returned deflation, with a minimum volume change set at 15 µl. Each recording session included 15-25 cycles
747 of inflation and deflation, with the first 5 cycles used for acclimation and excluded from the analysis. The
748 remaining cycles were used for data collection. Mice were habituated to the procedure for at least 3 days before
749 blood pressure measurements were recorded.

750 **Echocardiography**

751 Mice were anesthetized with 1.5% isoflurane (1.5% oxygen) and imaged in the supine position using Vevo 3100
752 Imaging System with a 35-MHz linear probe (Visualsonics, Canada). The core temperature was maintained at
753 37°C. Heart rates were kept consistent between the groups (400 – 450 bpm) (51). The heart was imaged in a
754 2D, short axis, and 4-chamber view by placing the pulsed wave Doppler at the septal corner of the mitral annulus.
755 Mitral inflow velocity (E) and longitudinal tissue velocity of the mitral anterior annulus (e') were measured through
756 Vevo2100 1.5.0 Image Software (52).
757
758 **Statistics**
759 Statistical analyses were performed using Prism software v8.4.1 (Graphpad, La Jolla, CA). The Pearson-
760 D'Agostino normality test was used to assess data distribution normality. When comparing two groups, two-tailed
761 Student's t-test with Welch's correction (unequal variances) was used. When comparing data for two or three
762 interacting variables, two-way and three-way ANOVA tests were used respectively. P value less than 0.05 was
763 considered significant. When the number of data points was less than 10, data were presented as single values
764 (dot plots, histograms). Analyses pooling data points over time were presented as line plots connecting means
765 and standard error of the mean.
766
767 **Study approval**
768 Mice were housed in a pathogen-free facility in accordance with the American Veterinary Medical Association
769 (AVMA) and under protocols fully approved by the Institutional Animal Care and Use Committee (IACUC) at
770 Cincinnati Children's Hospital Medical Center (#2022-0020, #2023-0002).
771
772 **Data availability**
773 RNA-seq and ChIP-seq datasets reported here are available on GEO as GSE252826, GSE252857,
774 GSE252856, GSE254114.
775
776

REFERENCES

1. Chen Y, Zhao X, and Wu H. Metabolic Stress and Cardiovascular Disease in Diabetes Mellitus: The Role of Protein O-GlcNAc Modification. *Arterioscler Thromb Vasc Biol.* 2019;39(10):1911-24.
2. De Rosa S, Arcidiacono B, Chiefari E, Brunetti A, Indolfi C, and Foti DP. Type 2 Diabetes Mellitus and Cardiovascular Disease: Genetic and Epigenetic Links. *Front Endocrinol (Lausanne).* 2018;9:2.
3. Jia G, DeMarco VG, and Sowers JR. Insulin resistance and hyperinsulinaemia in diabetic cardiomyopathy. *Nat Rev Endocrinol.* 2016;12(3):144-53.
4. Karwi QG, Sun Q, and Lopaschuk GD. The Contribution of Cardiac Fatty Acid Oxidation to Diabetic Cardiomyopathy Severity. *Cells.* 2021;10(11).
5. Schulze PC, Drosatos K, and Goldberg IJ. Lipid Use and Misuse by the Heart. *Circ Res.* 2016;118(11):1736-51.
6. Morrish NJ, Wang SL, Stevens LK, Fuller JH, and Keen H. Mortality and causes of death in the WHO Multinational Study of Vascular Disease in Diabetes. *Diabetologia.* 2001;44 Suppl 2:S14-21.
7. Oakley RH, Ren R, Cruz-Topete D, Bird GS, Myers PH, Boyle MC, et al. Essential role of stress hormone signaling in cardiomyocytes for the prevention of heart disease. *Proc Natl Acad Sci U S A.* 2013;110(42):17035-40.
8. Oster H, Damerow S, Kiessling S, Jakubcakova V, Abraham D, Tian J, et al. The circadian rhythm of glucocorticoids is regulated by a gating mechanism residing in the adrenal cortical clock. *Cell Metab.* 2006;4(2):163-73.
9. Wintzinger M, Panta M, Miz K, Prabakaran AD, Durumutla HB, Sargent M, et al. Impact of circadian time of dosing on cardiomyocyte-autonomous effects of glucocorticoids. *Mol Metab.* 2022;62:101528.
10. Sasse SK, Mailloux CM, Barczak AJ, Wang Q, Altonsy MO, Jain MK, et al. The glucocorticoid receptor and KLF15 regulate gene expression dynamics and integrate signals through feed-forward circuitry. *Mol Cell Biol.* 2013;33(11):2104-15.
11. Haldar SM, Jeyaraj D, Anand P, Zhu H, Lu Y, Prosdocimo DA, et al. Kruppel-like factor 15 regulates skeletal muscle lipid flux and exercise adaptation. *Proc Natl Acad Sci U S A.* 2012;109(17):6739-44.
12. Zhang L, Prosdocimo DA, Bai X, Fu C, Zhang R, Campbell F, et al. KLF15 Establishes the Landscape of Diurnal Expression in the Heart. *Cell Rep.* 2015;13(11):2368-75.

805 13. Haldar SM, Lu Y, Jeyaraj D, Kawanami D, Cui Y, Eapen SJ, et al. Klf15 deficiency is a molecular link
806 between heart failure and aortic aneurysm formation. *Sci Transl Med.* 2010;2(26):26ra.
807 14. Prosdocimo DA, Anand P, Liao X, Zhu H, Shelkay S, Artero-Calderon P, et al. Kruppel-like factor 15 is a
808 critical regulator of cardiac lipid metabolism. *J Biol Chem.* 2014;289(9):5914-24.
809 15. Prosdocimo DA, John JE, Zhang L, Efraim ES, Zhang R, Liao X, et al. KLF15 and PPARalpha
810 Cooperate to Regulate Cardiomyocyte Lipid Gene Expression and Oxidation. *PPAR Res.*
811 2015;2015:201625.
812 16. Sasse SK, Zuo Z, Kadiyala V, Zhang L, Pufall MA, Jain MK, et al. Response Element Composition
813 Governs Correlations between Binding Site Affinity and Transcription in Glucocorticoid Receptor Feed-
814 forward Loops. *J Biol Chem.* 2015;290(32):19756-69.
815 17. Holland WL, Xia JY, Johnson JA, Sun K, Pearson MJ, Sharma AX, et al. Inducible overexpression of
816 adiponectin receptors highlight the roles of adiponectin-induced ceramidase signaling in lipid and
817 glucose homeostasis. *Mol Metab.* 2017;6(3):267-75.
818 18. Keshvari S, Henstridge DC, Ng C, Febbraio MA, and Whitehead JP. Muscle-specific overexpression of
819 AdipoR1 or AdipoR2 gives rise to common and discrete local effects whilst AdipoR2 promotes
820 additional systemic effects. *Sci Rep.* 2017;7:41792.
821 19. Fernandez-Caggiano M, Kamynina A, Francois AA, Prysyazhna O, Eykyn TR, Krasemann S, et al.
822 Mitochondrial pyruvate carrier abundance mediates pathological cardiac hypertrophy. *Nat Metab.*
823 2020;2(11):1223-31.
824 20. Zhang Y, Taufalele PV, Cochran JD, Robillard-Frayne I, Marx JM, Soto J, et al. Mitochondrial pyruvate
825 carriers are required for myocardial stress adaptation. *Nat Metab.* 2020;2(11):1248-64.
826 21. Cluntun AA, Badolia R, Lettlova S, Parnell KM, Shankar TS, Diakos NA, et al. The pyruvate-lactate axis
827 modulates cardiac hypertrophy and heart failure. *Cell Metab.* 2021;33(3):629-48 e10.
828 22. Sakamuri S, Sperling JA, Sure VN, Dholakia MH, Peterson NR, Rutkai I, et al. Measurement of
829 respiratory function in isolated cardiac mitochondria using Seahorse XFe24 Analyzer: applications for
830 aging research. *Geroscience.* 2018;40(3):347-56.

831 23. Quattrocelli M, Wintzinger M, Miz K, Levine DC, Peek CB, Bass J, et al. Muscle mitochondrial
832 remodeling by intermittent glucocorticoid drugs requires an intact circadian clock and muscle PGC1α.
833 *Sci Adv.* 2022;8(7):eabm1189.
834 24. Quattrocelli M, Wintzinger M, Miz K, Levine DC, Peek CB, Bass J, et al. Muscle mitochondrial
835 remodeling by intermittent glucocorticoid drugs requires an intact circadian clock and muscle
836 PGC1alpha. *Sci Adv.* 2022;8(7):eabm1189.
837 25. Jiang Z, Elsarrag SZ, Duan Q, LaGory EL, Wang Z, Alexanian M, et al. KLF15 cistromes reveal a
838 hepatocyte pathway governing plasma corticosteroid transport and systemic inflammation. *Sci Adv.*
839 2022;8(10):eabj2917.
840 26. Cruz-Topete D, Oakley RH, Carroll NG, He B, Myers PH, Xu X, et al. Deletion of the Cardiomyocyte
841 Glucocorticoid Receptor Leads to Sexually Dimorphic Changes in Cardiac Gene Expression and
842 Progression to Heart Failure. *J Am Heart Assoc.* 2019;8(15):e011012.
843 27. Fisch S, Gray S, Heymans S, Haldar SM, Wang B, Pfister O, et al. Kruppel-like factor 15 is a regulator
844 of cardiomyocyte hypertrophy. *Proc Natl Acad Sci U S A.* 2007;104(17):7074-9.
845 28. Mori J, Patel VB, Abo Alrob O, Basu R, Altamimi T, Desaulniers J, et al. Angiotensin 1-7 ameliorates
846 diabetic cardiomyopathy and diastolic dysfunction in db/db mice by reducing lipotoxicity and
847 inflammation. *Circ Heart Fail.* 2014;7(2):327-39.
848 29. Alex L, Russo I, Holoborodko V, and Frangogiannis NG. Characterization of a mouse model of obesity-
849 related fibrotic cardiomyopathy that recapitulates features of human heart failure with preserved
850 ejection fraction. *Am J Physiol Heart Circ Physiol.* 2018;315(4):H934-H49.
851 30. Hafstad AD, Khalid AM, How OJ, Larsen TS, and Aasum E. Glucose and insulin improve cardiac
852 efficiency and postischemic functional recovery in perfused hearts from type 2 diabetic (db/db) mice.
853 *Am J Physiol Endocrinol Metab.* 2007;292(5):E1288-94.
854 31. Panagia M, Schneider JE, Brown B, Cole MA, and Clarke K. Abnormal function and glucose
855 metabolism in the type-2 diabetic db/db mouse heart. *Can J Physiol Pharmacol.* 2007;85(3-4):289-94.
856 32. Huynh K, Kiriazis H, Du XJ, Love JE, Jandeleit-Dahm KA, Forbes JM, et al. Coenzyme Q10 attenuates
857 diastolic dysfunction, cardiomyocyte hypertrophy and cardiac fibrosis in the db/db mouse model of type
858 2 diabetes. *Diabetologia.* 2012;55(5):1544-53.

859 33. Semeniuk LM, Kryski AJ, and Severson DL. Echocardiographic assessment of cardiac function in
860 diabetic db/db and transgenic db/db-hGLUT4 mice. *Am J Physiol Heart Circ Physiol.*
861 2002;283(3):H976-82.
862 34. Goncalves AC, Tank J, Diedrich A, Hilzendeger A, Plehm R, Bader M, et al. Diabetic hypertensive leptin
863 receptor-deficient db/db mice develop cardioregulatory autonomic dysfunction. *Hypertension.*
864 2009;53(2):387-92.
865 35. Mebrahtu TF, Morgan AW, West RM, Stewart PM, and Pujades-Rodriguez M. Oral glucocorticoids and
866 incidence of hypertension in people with chronic inflammatory diseases: a population-based cohort
867 study. *CMAJ.* 2020;192(12):E295-E301.
868 36. Gray S, Feinberg MW, Hull S, Kuo CT, Watanabe M, Sen-Banerjee S, et al. The Kruppel-like factor
869 KLF15 regulates the insulin-sensitive glucose transporter GLUT4. *J Biol Chem.* 2002;277(37):34322-8.
870 37. Tabebordbar M, Lagerborg KA, Stanton A, King EM, Ye S, Tellez L, et al. Directed evolution of a family
871 of AAV capsid variants enabling potent muscle-directed gene delivery across species. *Cell.*
872 2021;184(19):4919-38 e22.
873 38. Quattrocelli M, Wintzinger M, Miz K, Panta M, Prabakaran AD, Barish GD, et al. Intermittent prednisone
874 treatment in mice promotes exercise tolerance in obesity through adiponectin. *J Exp Med.* 2022;219(5).
875 39. Saito M, and Bray GA. Diurnal rhythm for corticosterone in obese (ob/ob) diabetes (db/db) and gold-
876 thioglucose-induced obesity in mice. *Endocrinology.* 1983;113(6):2181-5.
877 40. Zelikovich AS, Joslin BC, Casey P, McNally EM, and Ajroud-Driss S. An Open Label Exploratory Clinical
878 Trial Evaluating Safety and Tolerability of Once-Weekly Prednisone in Becker and Limb-Girdle Muscular
879 Dystrophy. *J Neuromuscul Dis.* 2022;9(2):275-87.
880 41. Lamia KA, Papp SJ, Yu RT, Barish GD, Uhlenhaut NH, Jonker JW, et al. Cryptochromes mediate
881 rhythmic repression of the glucocorticoid receptor. *Nature.* 2011;480(7378):552-6.
882 42. Nader N, Chrousos GP, and Kino T. Circadian rhythm transcription factor CLOCK regulates the
883 transcriptional activity of the glucocorticoid receptor by acetylating its hinge region lysine cluster:
884 potential physiological implications. *FASEB J.* 2009;23(5):1572-83.
885 43. Holland WL, Miller RA, Wang ZV, Sun K, Barth BM, Bui HH, et al. Receptor-mediated activation of
886 ceramidase activity initiates the pleiotropic actions of adiponectin. *Nat Med.* 2011;17(1):55-63.

887 44. Field BC, Gordillo R, and Scherer PE. The Role of Ceramides in Diabetes and Cardiovascular Disease
888 Regulation of Ceramides by Adipokines. *Front Endocrinol (Lausanne).* 2020;11:569250.
889 45. Yazici D, and Sezer H. Insulin Resistance, Obesity and Lipotoxicity. *Adv Exp Med Biol.* 2017;960:277-
890 304.
891 46. Wende AR, Schell JC, Ha CM, Pepin ME, Khalimonchuk O, Schwertz H, et al. Maintaining Myocardial
892 Glucose Utilization in Diabetic Cardiomyopathy Accelerates Mitochondrial Dysfunction. *Diabetes.*
893 2020;69(10):2094-111.
894 47. McCommis KS, Kovacs A, Weinheimer CJ, Shew TM, Koves TR, Ilkayeva OR, et al. Nutritional
895 modulation of heart failure in mitochondrial pyruvate carrier-deficient mice. *Nat Metab.*
896 2020;2(11):1232-47.
897 48. Vadvalkar SS, Matsuzaki S, Eyster CA, Giorgione JR, Bockus LB, Kinter CS, et al. Decreased
898 Mitochondrial Pyruvate Transport Activity in the Diabetic Heart: ROLE OF MITOCHONDRIAL
899 PYRUVATE CARRIER 2 (MPC2) ACETYLATION. *J Biol Chem.* 2017;292(11):4423-33.
900 49. Rana S, Prabhu SD, and Young ME. Chronobiological Influence Over Cardiovascular Function: The
901 Good, the Bad, and the Ugly. *Circ Res.* 2020;126(2):258-79.
902 50. Prabakaran AD, McFarland K, Miz K, Durumutla HB, Piczer K, El Abdellaoui Soussi F, et al. Intermittent
903 glucocorticoid treatment improves muscle metabolism via the PGC1alpha/Lipin1 axis in an aging-
904 related sarcopenia model. *J Clin Invest.* 2024;134(11).
905 51. Schnelle M, Catibog N, Zhang M, Nabeebaccus AA, Anderson G, Richards DA, et al.
906 Echocardiographic evaluation of diastolic function in mouse models of heart disease. *J Mol Cell Cardiol.*
907 2018;114:20-8.
908 52. Jeong EM, Chung J, Liu H, Go Y, Gladstein S, Farzaneh-Far A, et al. Role of Mitochondrial Oxidative
909 Stress in Glucose Tolerance, Insulin Resistance, and Cardiac Diastolic Dysfunction. *J Am Heart Assoc.*
910 2016;5(5).
911